RADC-TR-76-275
Semiannual Technical Report No. 3
1 February 1976

INFRARED RESPONSE OF IMPURITY DOPED SILICON MOSFET'S (IRFET'S): FABRICATION AND CHARACTERIZTION OF THE GALLIUM DOPED INFRARED SENSING MOSFET

University of Arkansas

Sponsored by
Defense Advanced Research Projects Agency
ARPA Order No. 2794

ROME AIR DEVELOPMENT CENTER
AIR FORCE SYSTEMS COMMAND
GRIFFISS AIR FORCE BASE, NEW YORK 13441

This report has been reviewed by the RADC Information Office (OI) and is releasable to the National Technical Information Service (NTIS). At NTIS it will be releasable to the general public, including foreign nations.

This technical report has been reviewed and is approved.

Jacques E. Ludman

JACQUES E. LUDMAN
Contract Monitor

Unclassified

SECURITY CLASSIFICATION OF THIS PAGE (When Data Entered)

(19) REPORT DOCUMENTATION PAGE		READ INSTRUCTIONS BEFORE COMPLETING FORM
1. REPORT NUMBER (18) RADC-TR-76-275	2. GOVT ACCESSION NO.	3. RECIPIENT'S CATALOG NUMBER
4. TITLE (and Subtitle) (6) Infrared Response of Impurity Doped Silicon MOSFET's (IRFET's): Fabrication and Characterization of the Gallium Doped Infrared Sensing MOSFET.		5. TYPE OF REPORT & PERIOD COVERED (9) Semiannual Technical Rept. no. 3, 1 Aug. 75- 1 Feb. 76,
		6. PERFORMING ORG. REPORT NUMBER
7. AUTHOR(s) (10) Leonard Forbes Bainer Hall, Dept. of Electrical Engineering University of California, Davis Davis, California 95616		8. CONTRACT OR GRANT NUMBER(s) (15) F19628-75-C-0071, ARPA Order-2794
9. PERFORMING ORGANIZATION NAME AND ADDRESS Board of Trustees University of Arkansas dept EE Fayetteville, Arkansas 72701		10. PROGRAM ELEMENT, PROJECT, TASK AREA & WORK UNIT NUMBERS 61101E 563801-01
11. CONTROLLING OFFICE NAME AND ADDRESS Defense Advanced Research Projects Agency 1400 Wilson Blvd. Arlington, VA 22209		12. REPORT DATE (11) 1 February 1976 13. NUMBER OF PAGES 88 (12) 94 p.
14. MONITORING AGENCY NAME & ADDRESS (if different from Controlling Office) Deputy for Electronic Technology (RADC(ETSD)), Hanscom AFB, MA 01731 Monitor/Jacques E. Ludman/ETSD		15. SECURITY CLASS. (of this report) Unclassified 15a. DECLASSIFICATION/DOWNGRADING SCHEDULE

16. DISTRIBUTION STATEMENT (of this Report)

Approved for public release: distribution unlimited

17. DISTRIBUTION STATEMENT (of the abstract entered in Block 20, if different from Report)

18. SUPPLEMENTARY NOTES

This research was sponsored by the Defense Advanced Research Projects Agency, ARPA Order No. 2794

19. KEY WORDS (Continue on reverse side if necessary and identify by block number)

Extrinsic silicon infrared detectors.

20. ABSTRACT (Continue on reverse side if necessary and identify by block number)

Fabrication and characterization of the gallium doped infrared sensing MOSFET is described.
Gallium doped MOSFET device structures have been fabricated by diffusion of gallium from doped oxide sources into n-channel MOSFET's fabricated on a normal boron doped p-type substrates.

CONTINUED

DD FORM 1 JAN 73 1473 EDITION OF 1 NOV 65 IS OBSOLETE

Unclassified

SECURITY CLASSIFICATION OF THIS PAGE (When Data Entered)

409489 DN

The process developed produces double doped, both gallium and boron substrates.

The characteristics of the gallium impurity center in silicon have been determined by measurements on the MOSFET device structure, and specifically the thermal emission rate of holes from neutral gallium centers determined. To the best of the author's knowledge the emission rate of gallium has not been previously measured. A very significant field enhancement has been observed in this thermal emission rate and is described by the Poole-Frenkel effect.

Measurements have been made of the characteristics of the gallium doped MOSFET (IRFET) as an infrared detector. It has been found that the device operated according to previously published models and design criteria and in a manner consistent with that previously observed for the indium and gold doped devices.

These results demonstrate that the gallium doped infrared sensing MOSFET (IRFET) will operate in the far infrared, 8 to 14 micrometer wavelength range, and as such might be particularly suited to large scale integrated infrared imaging arrays and applications.

TECHNICAL REPORT SUMMARY**

The gallium diffusion process from Emulsitone doped oxide sources was developed using MOS capacitor structures. The process was then modified and applied to MOSFET device structures by doing the gallium diffusion after or during gate oxidation.

These latter MOSFET devices were then characterized in a low temperature cryo-tip in the range 20 to 50 °K. A rather significant field enhancement was observed in the thermal emission rate of the gallium center in silicon, the longest time constant observed being of the order 1.0 second at 20 °K. Detailed measurements were made of the change in transistor characteristics due to thermal emission or optical emission of holes from the gallium centers due to incident infrared radiation. The response characteristics correspond to the model previously developed for the infrared sensing MOSFET(IRFET) and are consistent with previous measurements on indium and gold doped devices.

Responsivities of the order of 25 milliwatts/microjoule have been readily observed in non-optimum device structures and the transistor characteristics have been found to be relatively insensitive to temperature in the range 20 to 30 °K.

More work remains to be done in obtaining more optimum device structures, detailed spectral response characteristics, and investigating uniformity of response.

** This report is based on an MSEE Thesis submitted to the Department of Electrical Engineering, University of Arkansas, by Hamman ElAbd.

TABLE OF CONTENTS

I. INTRODUCTION

This thesis describes the effect of infrared radiation on the gallium impurity centers in the surface depletion region of a metal-oxide-silicon field effect transistor (MOSFET).

The research objectives were to measure the thermal emission rate dependance on temperature, the charge state device characteristics and the optical emission rate-wave length dependance in the far infrared region (8 to 14 micrometer wavelength).

Gallium-doped MOSFETs were designed and fabricated in the University of Arkansas Solid-State Devices Laboratory. The fabrication processes for the gallium doped MOS capacitor and MOS field effect transistor are described in the first chapter of this thesis. We did not spend much time on the Ga. doped MOS-C, but used it mostly to determine if we were getting enough gallium into the fabricated device, i.e. the MOS-C was used as a process monitor. In other words, the objective was to compare the theoretical and experimental characteristic of the high frequency capacitance-voltage (C-V) curves, and deduce from this the total impurity concentration at the surface of the wafers. The gallium and boron concentrations were determined from the low temperature measurements on the gallium-boron doped MOSFETs.

The key issue in the fabrication process of Ga-B doped MOSFET was to ensure satisfactory gallium concentration in the end-device by preventing the gallium atoms from escaping from the Si-surface into the atmosphere during predeposition or thermal oxidation.

The thermal and optical response of the gallium centers could only be observed at low temperatures. Satisfactory time constants were measured

in the temperature range 21°K to 50°K. The device was mounted in a liquid hydrogen cooled refrigerator. Operation at the lower end of the temperature range was only possible when the thermal load on the cryotip was reduced to a minimum.

To minimize the 300°K background radiation which peaks in the device response range, the IR filter was placed inside the cryogenic refrigerator (cold filter operation). The IR filter was attached to the radiation shield of the cryogenic refrigerator, which is held at liquid nitrogen temperature.

The thermal and charge state device characteristics enabled us to preliminarily study the electric field effect of the re-emission of the trapped holes in the gallium centers. This effect is well explained by a lowering of the Coulomb potential barrier about the gallium centers [8,9] (the Poole-Frenkel effect).

The operation of the infrared sensing MOSFET (IRFET) can be analyzed using the well known MOSFET equations [2]. The experimental results were found in most cases, to verify the model equations and with an accuracy sufficient for most engineering applications. Although the device is designed to operate as a photon detector in the 8 to 14 micrometer wavelength range, the activation energy of the gallium center; calculated from the thermal response data, suggests that the gallium center should respond to photon energies from 1 micrometer in the near infrared and up to 41 micrometer wavelength in the far infrared range.

The double doped Si-IR sensing MOSFET is characterized by negative photoconductivity, high responsivity, integrating function and static ROM capability.

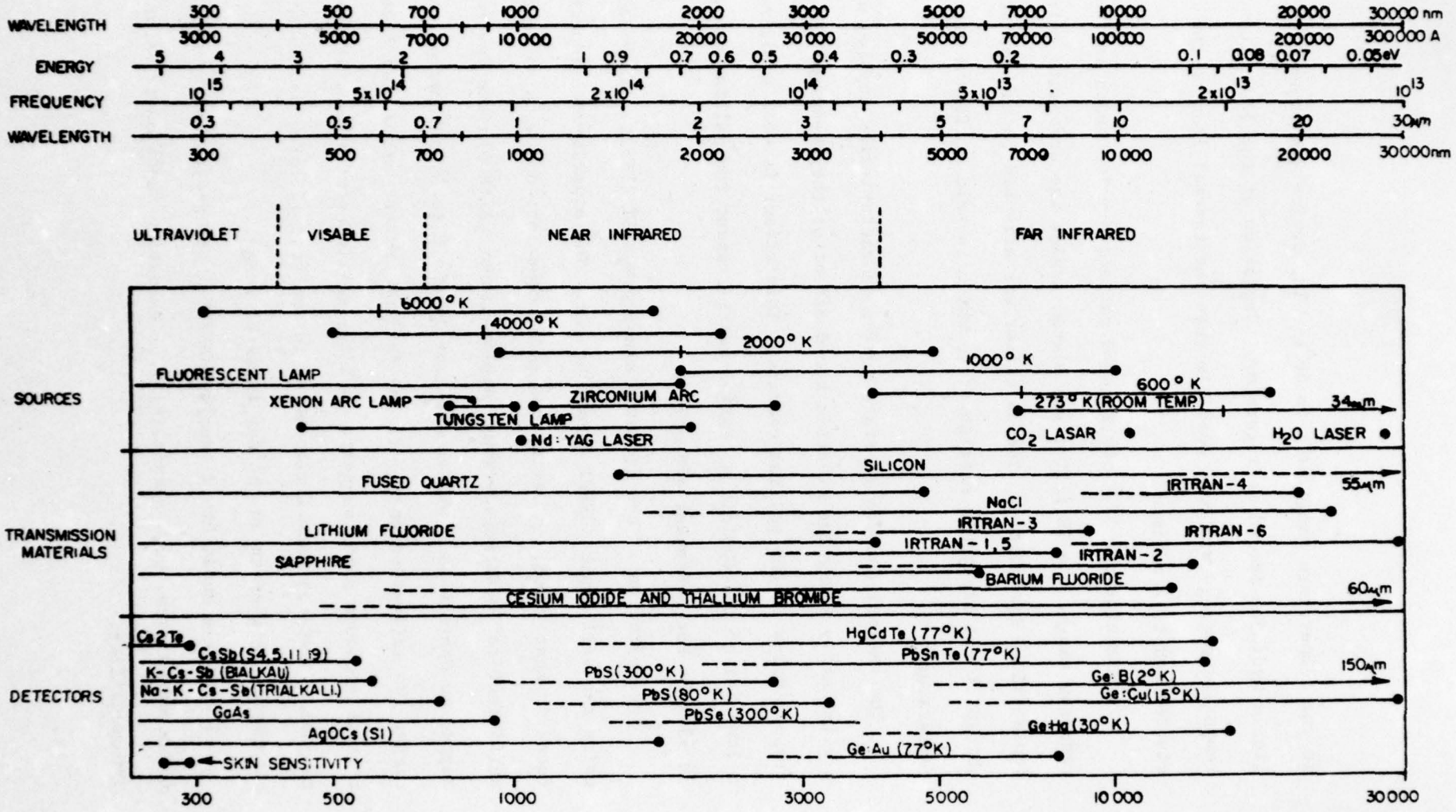

TABLE I: INFRARED DETECTORS, TRANSMISSION MATERIALS AND SOURCES

ELECTRONICS February 1972

Considerable amount of research has recently been reported on extrinsic silicon infrared detectors [1,2,3,4,5,6,7] because of the obvious benefits obtained by employing the silicon technology. Table 1 shows tha available IR detectors, transmission materials and sources and their location in the IR spectrum.

II. GALLIUM DOPING BY DIFFUSION FROM DOPED OXIDE SOURCES

Gallium diffusion differs from the conventional diffusion process (such as boron and phosphorus) encountered in semiconductor manufacturing in that gallium out-diffuses rapidly when silicon is thermally oxidized, and silicon dioxide does not mask gallium [10]. The diffusion constant of gallium in SiO_2 is estimated to be a factor of 625 greater than its diffusion constant in silicon at 1200°C [10]. The SiO_2 is therefore transparent to the gallium for practical purposes. The diffusion constant of gallium in silicon is approximately four times that of boron at the same temperature.

The objective of this section of the study was to establish a process for producing double doped (gallium and boron) n-channel MOSFET's. The approach was to begin with p-type boron wafers and diffuse phosphorus for the source and drain regions and gallium in the channel region under the gate. Gallium doping by diffusion from doped oxide sources was carried out at the last phase of the MOSFET fabrication process. A liquid diffusion source (gallium silicafilm) is spun over the entire wafer. The wafer is allowed to dry then subjected to a predeposition drive-in cycle. It was found that the gallium is violatile at high temperatures and the wafers must be stacked during predeposition to prevent out diffusion.

According to the manufacturer [11], the source produces a co-error function distribution for predeposition time up to one hour. After predeposition, the gallium silicafilm is removed by etching and a drive-in step is performed to bring down the surface concentration somewhat and produce a deeper more uniform diffusion profile.

To insure that gallium does not invert the source and drain regions, a phosphorus source with a surface concentration higher than the solid solubility of gallium is used. The phosphorus source concentration was $10^{21}/cm^3$, which is higher than the maximum value of gallium solid solubility $4 \times 10^{19} cm^{-3}$ observed at 1250°C. Two different gallium source concentrations were used $10^{19} cm^{-3}$ and $10^{17} cm^{-3}$. The resulting total doping concentration was $2.25 \times 10^{16} cm^{-3}$. The calculated gallium concentration was $0.45 \times 10^{16} cm^{-3}$.

The MOSFET's were produced on 2 ohm-cm (100) orientation boron doped substrate. The channel W/L ratio is 8.17. The gate oxide estimated by viewing the oxide perpendicularly under white light and varified by the C-V measurements was around 7000A°.

The section below describes the experiments performed and the results in establishing the gallium process.

A. VERIFICATION OF GALLIUM DOPING

Many MOS capacitors were fabricated on P and N-type silicon wafers. Gallium was predeposited on the wafer surface for various periods of time. Also the drive in diffusion period was varied. The oxide thickness was varied between 2000A°, 3000A°, and 4000A°. The gallium diffusion in the Si wafer was observed with satisfactory concentrations.

The object wafer was stacked between two buffer n-type wafers during the predeposition and drive-in periods, to prevent gallium from escaping the surface during heat treatment.

Gallium diffusion was performed from a $10^{19} cm^{-3}$ source into a group of $10^{16} cm^{-3}$ phosphorus doped N-type Si wafers. The result of this

experiment was a definite surface inversion; verified by measuring the capacitance characteristics of the capacitor versus voltage. The C-V characteristics corresponded to p-type surface instead of an N-type surface, see Fig. 1.

From the recorded C-V characteristics of the MOS capacitor, Fig. 1, and from the normalized minimum capacitance versus oxide thickness for ideal MIS diodes under high frequency condition, Fig. 2; determination of the wafer doping after gallium diffusion was possible [10].

$$\frac{C_{min}}{C_i} = \frac{C_{min}}{C_{max}} = \frac{118}{125} = 0.944 \qquad (1)$$

The oxide thickness can be determined from

$$C_{max} = C_{ox} = \varepsilon\varepsilon_r \frac{A}{d_{ox}} \qquad (2)$$

where, C_{ox} stands for oxide capacitance; A stands for area; d_{ox} stands for oxide thickness; and $\varepsilon\varepsilon_r$ stands for the electric permittivity.

The capacitor had a diameter of 40 mils and an area of ($8.107 \times 10^{-3} cm^2$), thus;

$$d_{ox} \simeq \frac{2.83 \times 10^{-15}}{C_{ox}} = 2260A^{o} \qquad (3)$$

and from Fig. 2, the doping is

$$N_A \simeq 10^{18} cm^{-3}. \qquad (4)$$

Since the original substrate doping was less than $10^{16} cm^{-3}$; then we conclude that the resultant gallium doping is around $10^{18} cm^{-3}$.

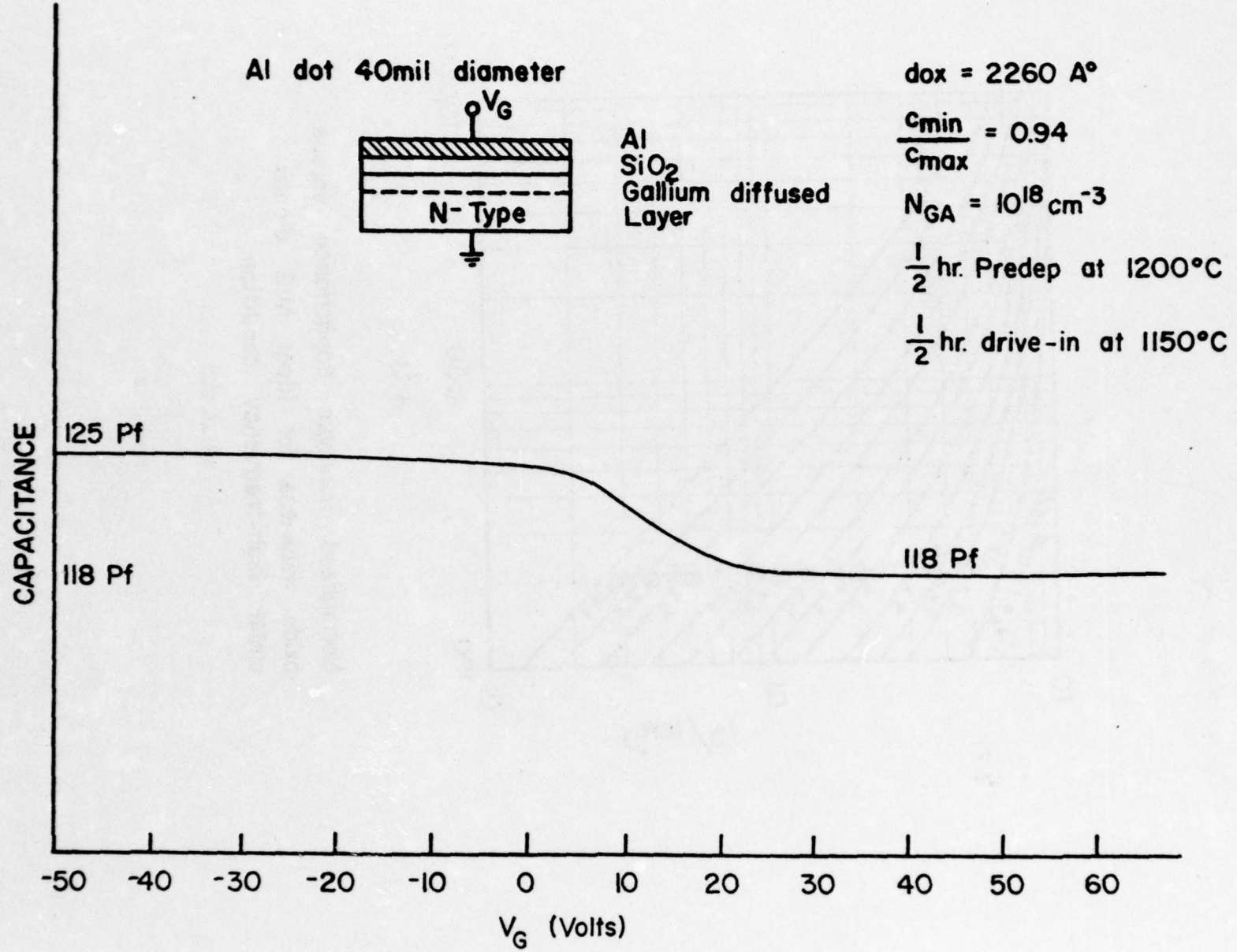

Fig. 1: C-V CURVE OF AN MOS CAPACITOR

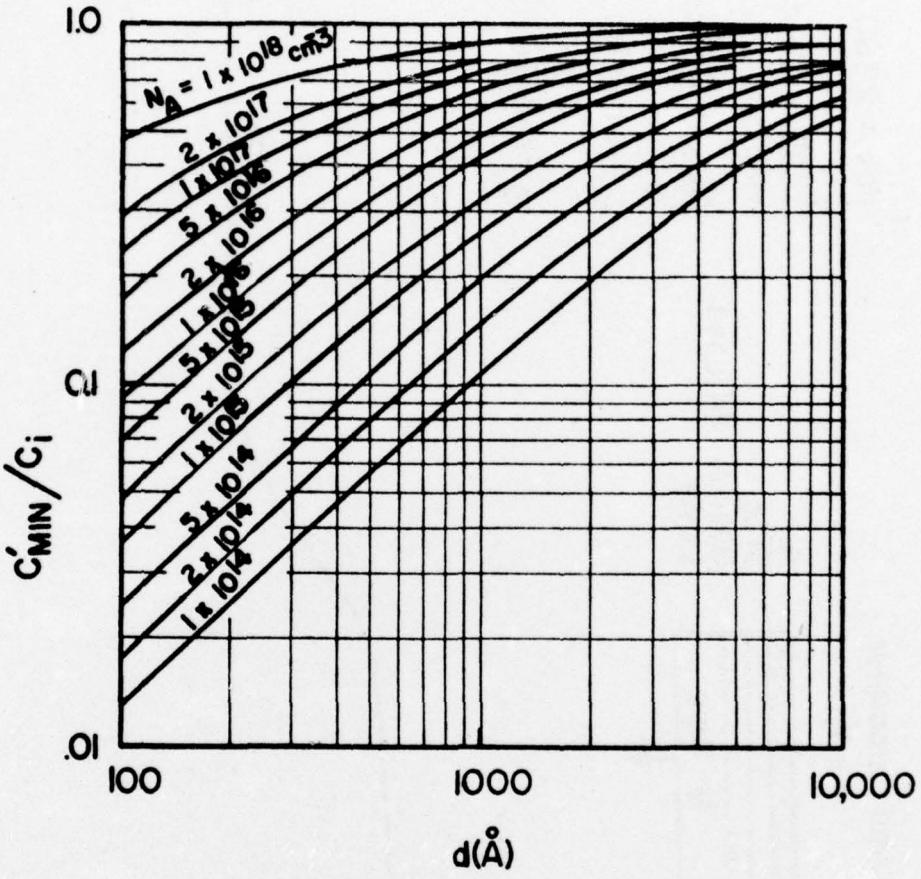

Normalized minimum capacitance versus oxide thickness for ideal MIS diodes under high-frequency condition.

AFTER SZE [12]

FIGURE 2

B. GALLIUM DIFFUSION PROCESS FOR p-TYPE WAFERS

The following is a description of the fabrication procedure of MOS capacitors and MOSFET's on p-type silicon substrates.

B.1 Fabrication of MOS Capacitors (Boron, Gallium)

The following is a description of the fabrication procedure for MOS capacitors.

1. Oxide growth (4000A° SiO_2) - See Fig. (3).

   The p-type Silicon Wafer is processed as follows in the oxidation furnace.

   a) 20 Minutes dry oxidation at 1100°c.

   b) 60 Minutes wet oxidation at 1100°c.

   c) 20 Minutes dry oxidation at 1100°c.

   d) 30 Minutes aneal in N_2 at 1100°c.

2. Coat with Gallium Silicafilm - See Fig. (4).

   The wafer is placed on the spinner. Eight drops of Gallium Silicafilm are depositied on the wafer while spinning at 3000 rpm for ten seconds.

   The film is left to dry at room temperature for one hour.

3. Gallium Diffusion - See Fig. (5) and (6).

   The wafers are stacked and placed in the diffusion furnace; in a pure N_2 ambient.

   a) Predeposition--30 minutes at 1200°c.

   b) Remove the Gallium Silicafilm by etching in a buffer solution (1:4 HF:NH4F) for one to one and a half minutes.

   c) Drive in diffusion--60 minutes at 1150°c.

4. Metalization and photolithography to obtain a capacitor with a guard ring for surface accumulation-See Fig. (7).

First Step

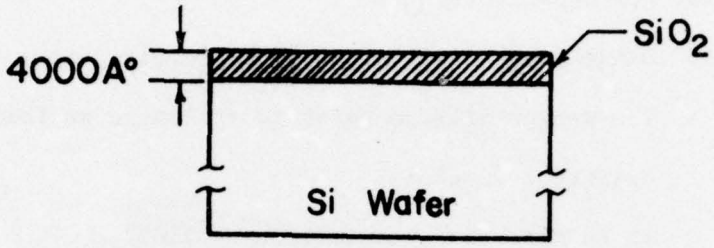

FIGURE 3

Second Step

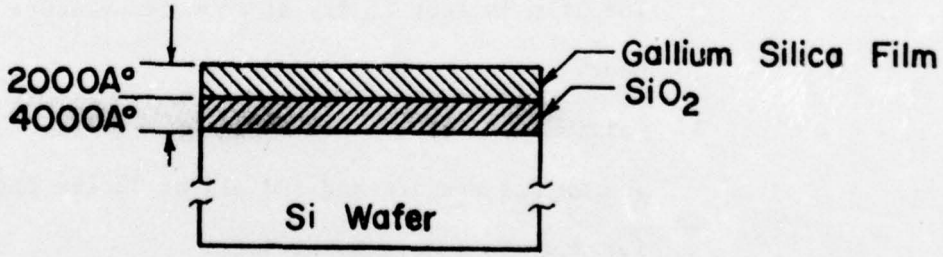

FIGURE 4

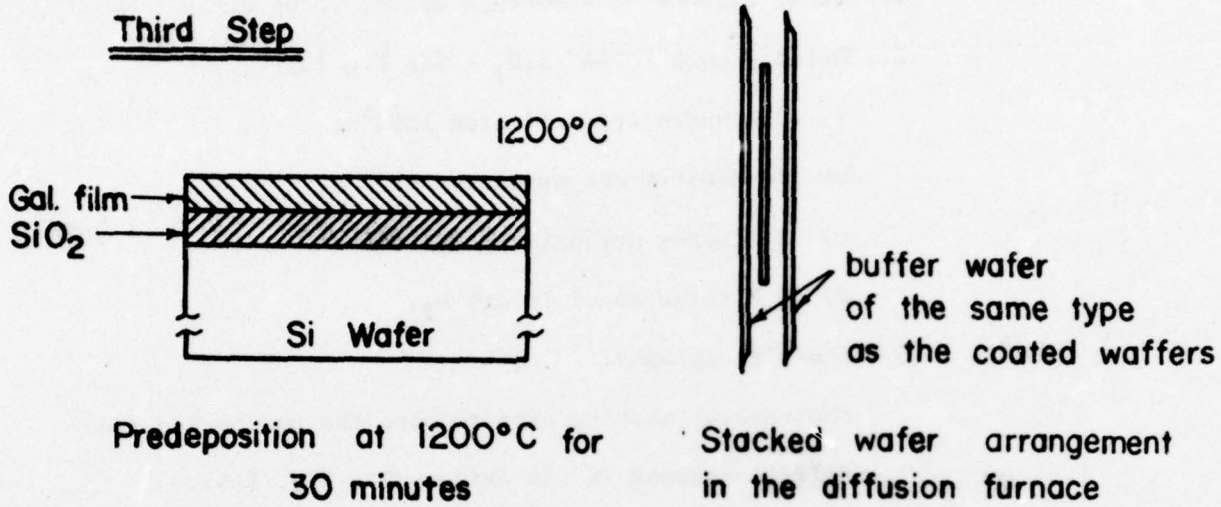

Predeposition at 1200°C for 30 minutes

Stacked wafer arrangement in the diffusion furnace

FIGURE 5

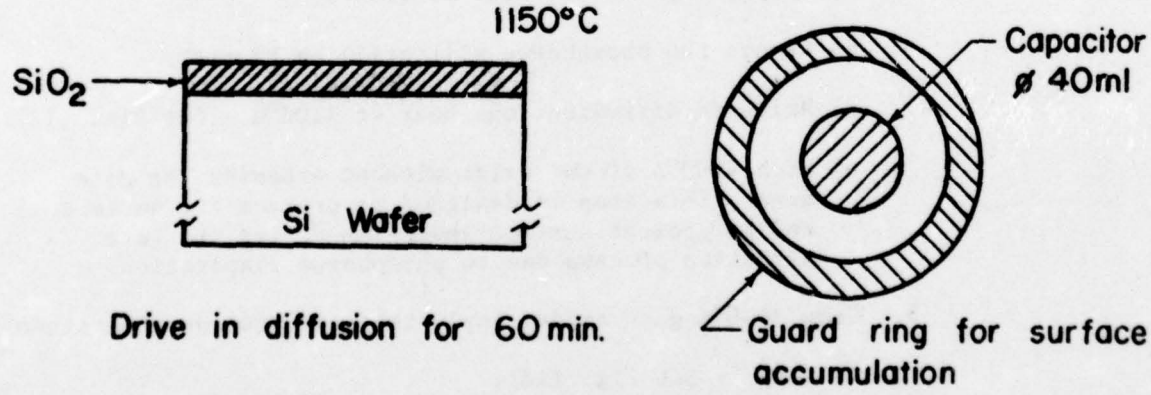

Drive in diffusion for 60 min.

FIGURE 6

FIGURE 7

B.2 Fabrication of Double Doped, MOS-FET (Boron, Gallium):

The following is a description of the manufacturing procedure for MOSFET's.

1. Clean surface of Si-p-type wafer, Boron doped - See Fig. (8).
2. Oxide growth 7000A° SiO_2 - See Fig.(9).
   a) 20 Minutes dry oxidation 1100°c.
   b) 180 Minutes wet oxidation 1100°c.
   c) 20 Minutes dry oxidation 1100°c.
   d) 30 Minutes aneal in dry N_2.
3. Photolithography:

   Photoresist masking step to open the source and drain diffusion areas in the oxide - See Fig. (10).
4. Phosphorus diffusion: See Fig. (11).
   a) Coat the surface of the wafer with phosphorus silicafilm. Deposit 5 drops of phosphorus silicafilm on the surface of the wafer while spinning at 3000 rpm for ten seconds. (This process is repeated two times). The wafer is then baked at 200°c for 15 minutes to dry the phosphorus film.
   b) Predeposition: one hour at 1100°c.
   c) Remove the phosphorus silicafilm by HF etch.
   d) Drive in diffusion: one hour at 1100°c - See Fig. (12).
   e) Etch 4000°A of the oxide without exposing the gate area. This step is designed to protect the surface and to prevent surface inversion during the gate oxidation process due to phosphorus evaporation.
5. Grow 3000°A gate oxide: Apply the same procedure outlined in Step 2. See Fig. (13).
6. Photolithography:

   Photoresist masking step to open the contact holes in the oxide of the source and drain regions - See Fig. (14).

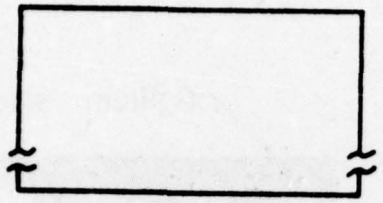

P-type Si Wafer
(Boron doped)

FIGURE 8

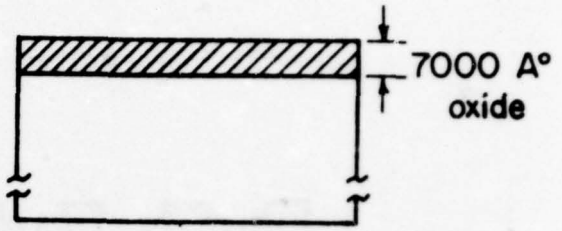

oxide growth

FIGURE 9

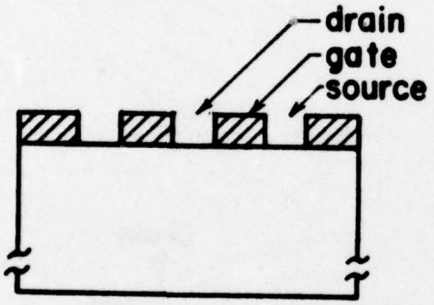

Opening the source
and drain regions
in the oxide.

FIGURE 10

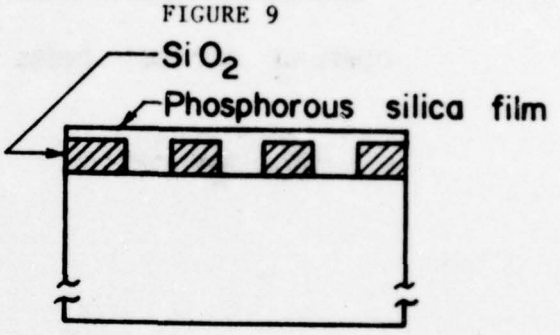

FIGURE 11

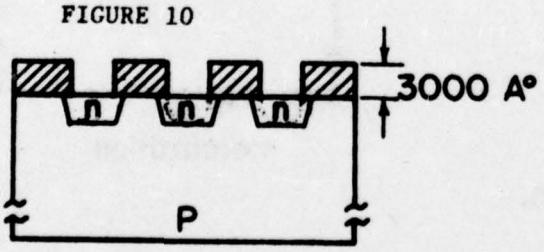

source & drain
regions

FIGURE 12

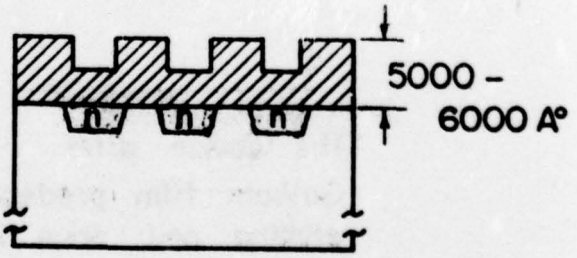

gate oxide

FIGURE 13

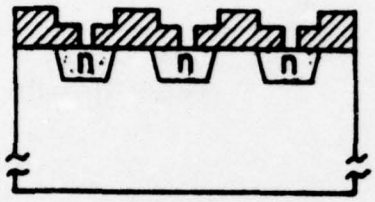

opening contact holes

FIGURE 14

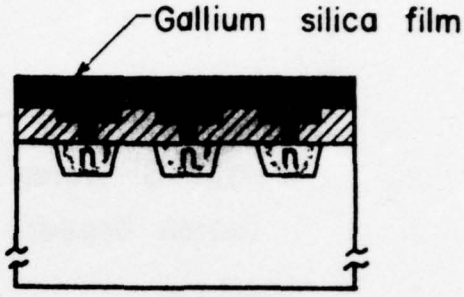

FIGURE 15

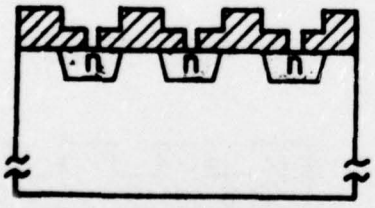

the device after
Gallium film predeposition,
etching and drive in

FIGURE 16

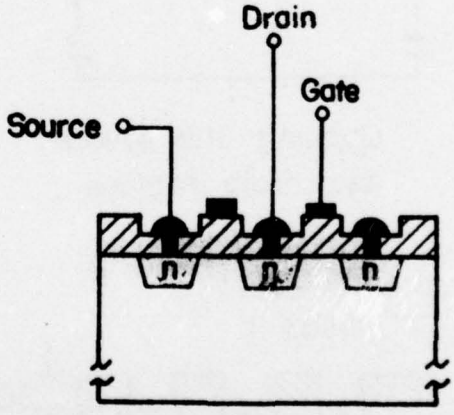

metalization

FIGURE 17

7. Gallium Diffusion: (see Fig. (15).

   a) Deposit 8 drops of the Gallium silicafilm on the surface of the wafer while spinning at 3000 rpm for ten seconds.

   b) Dry the gallium film at room temperature for one hour.

   c) Predeposition: 30 Minutes at 1200°c.

   d) Etch the silicafilm.

   e) Drive in diffusion: 60 Minutes at 1150°c in dry N_2 ambient.

8. Etch 700A° of SiO_2 from the surface to remove any oxide formed in the contact holes.

9. Metalization and photolithography to establish separate contacts with source, drain regions and gate oxide.

B.3 An Improved Process for the Fabrication of Double Doped MOSFET

The MOSFET fabrication process as described in Section B.2 yields devices with varying gate oxide thickness on the same wafer. This is due to the exposure of the entire wafer to two etching steps after the gate oxide growth. However, by combining the gate oxide growth and gallium drive-in within a step, the gate oxide uniformity can be preserved. In this case the gate oxide growth was carried out as follows:

15 min. dry oxidation

60 min. wet oxidation

20 min. N_2 aneal

Sulfuric acid was used to remove any remaining gallium at the surface of the wafer after the etching step of the gallium silicafilm. This was found to enhance considerably the yield of the process, by reducing the number of gate shorts.

Therefore, by advancing the gallium diffusion process to immediately follow the phosphorus diffusion, by using sulfuric acid wash after Ga silicafilm etch and by combining the gate oxide growth and gallium drive-in within a step a considerable improvement in the process yield and in the uniformity of device characteristics can be obtained.

C. Gallium Doped MOSFET At Room Temperature

The MOSFET's that were fabricated according to the process described above, were mounted and measured at room temperature. The I-V characteristics of one of them is shown in Fig. (18). By measuring the threshold voltage at various back gate voltages, the Ga concentration was estimated to be $\simeq 10^{17} cm^{-3}$.

Two MOSFET devices were selected for low temperature measurements, Device A and B. The dependence of threshold voltage on back gate bias at room temperature (Fig. 19) enabled us to deduce the total substrate doping.

The slope of the lines in Fig. 19 =

$$\frac{dV_T}{d(\sqrt{1 + V_{BG}})} = \sqrt{\frac{2\kappa_{si} C_o q N_{sub}}{C_o}} \qquad (5)$$

from equation (5) and Fig. 19 we determined that the total substrate doping is $2.25 \times 10^{16}/cm^3$ for device A, and $1.4 \times 10^{17}/cm^3$ for device B.

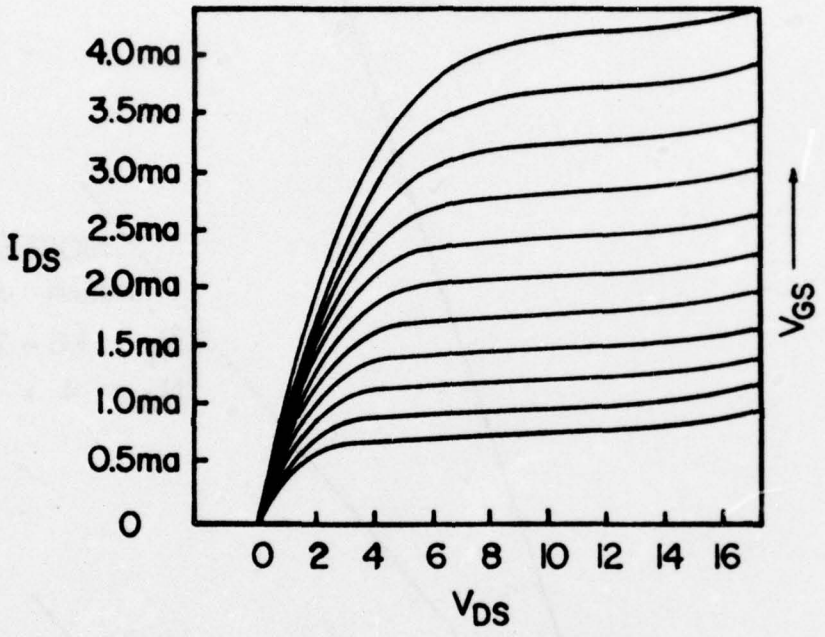

Double doped MOSFET
(Gallium - Boron)

Fig. 18

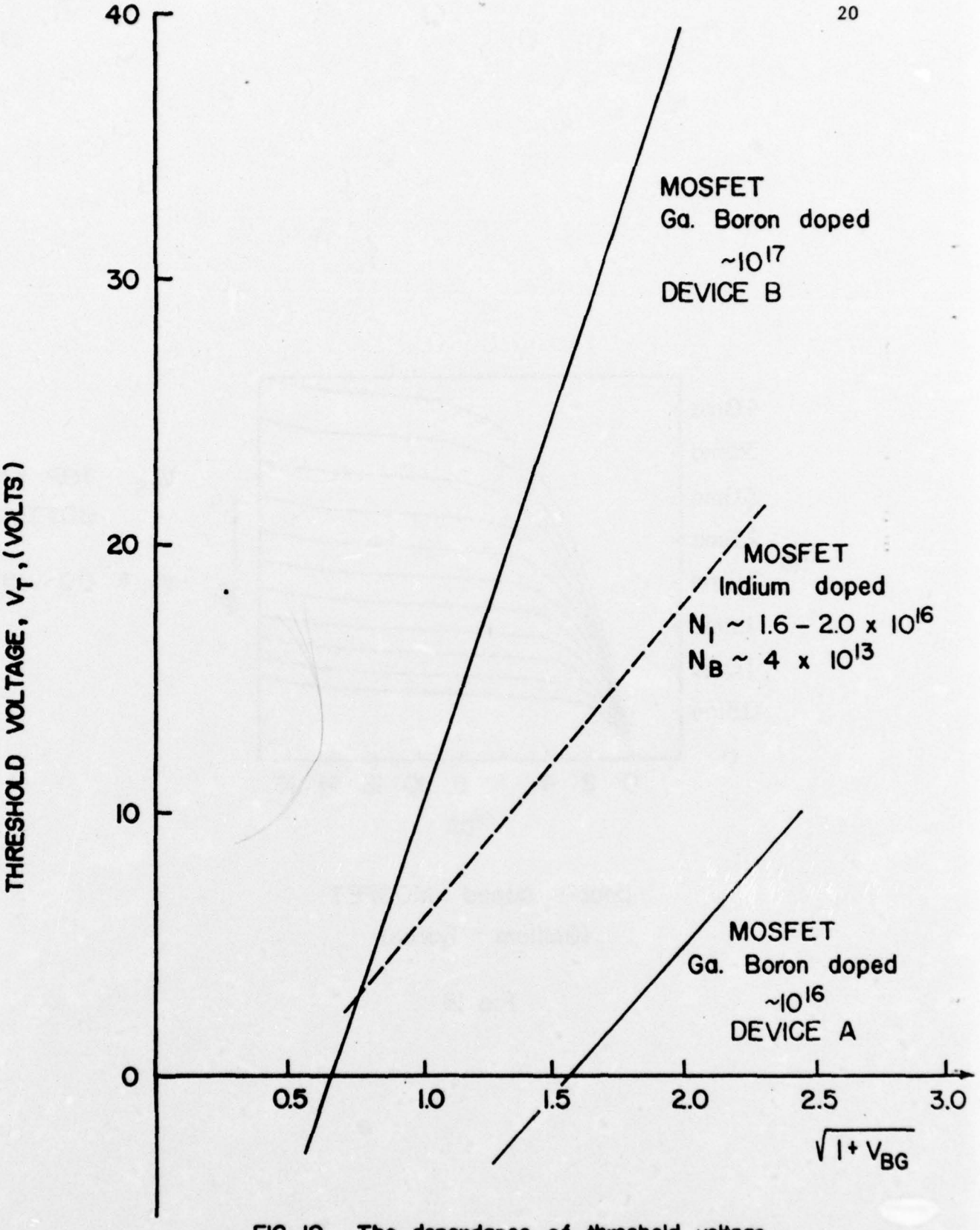

FIG. 19. The dependance of threshold voltage on back-gate bias at room temperature

III. DEVICE OPERATION

Gallium doping introduces an acceptor level in the silicon band gap. The energy level of the gallium center is shown in Figure 20. The ionization energy E_i of the gallium center is a measure of the energy required to release a hole to the valence energy band.

Gallium is an impurity from group III of the periodic table, which requires an extra electron to complete the valence bonding requirements [13]. The gallium center receives the extra electron from the neighboring silicon atoms and thereby create holes. The ionization energy of the gallium center in silicon has been determined by Hall measurements [14,15, 16,17]. In this case, the density of the thermally liberated hole which is inversly proportional to the Hall constant, has a temperature dependance of the form $\exp(-E_i/KT)$, where K is the Boltzmann's constant and T is the absolute temperature [18]. The gallium ionization energy was found to be 0.065eV [16]. The gallium ionization energy was also determined [19,20] by an optical method. The minimum infrared photon energy required to cause the ionization of the gallium center at low temperatures was measured [19] and found to be 0.071eV. This small ionization energy for gallium in silicon necessitates very low temperatures of operation.

Throughout the quoted work [14,15,16,17,18,19,20] the author has found no reference to the effect of the electric field on these measured values of the ionization energies for gallium in silicon or for any of the other shallow acceptors that were under investigation. Therefore, the above quoted values for the gallium ionization energy should not be compared to the values we calculated fro the activation energy of the gallium centers.

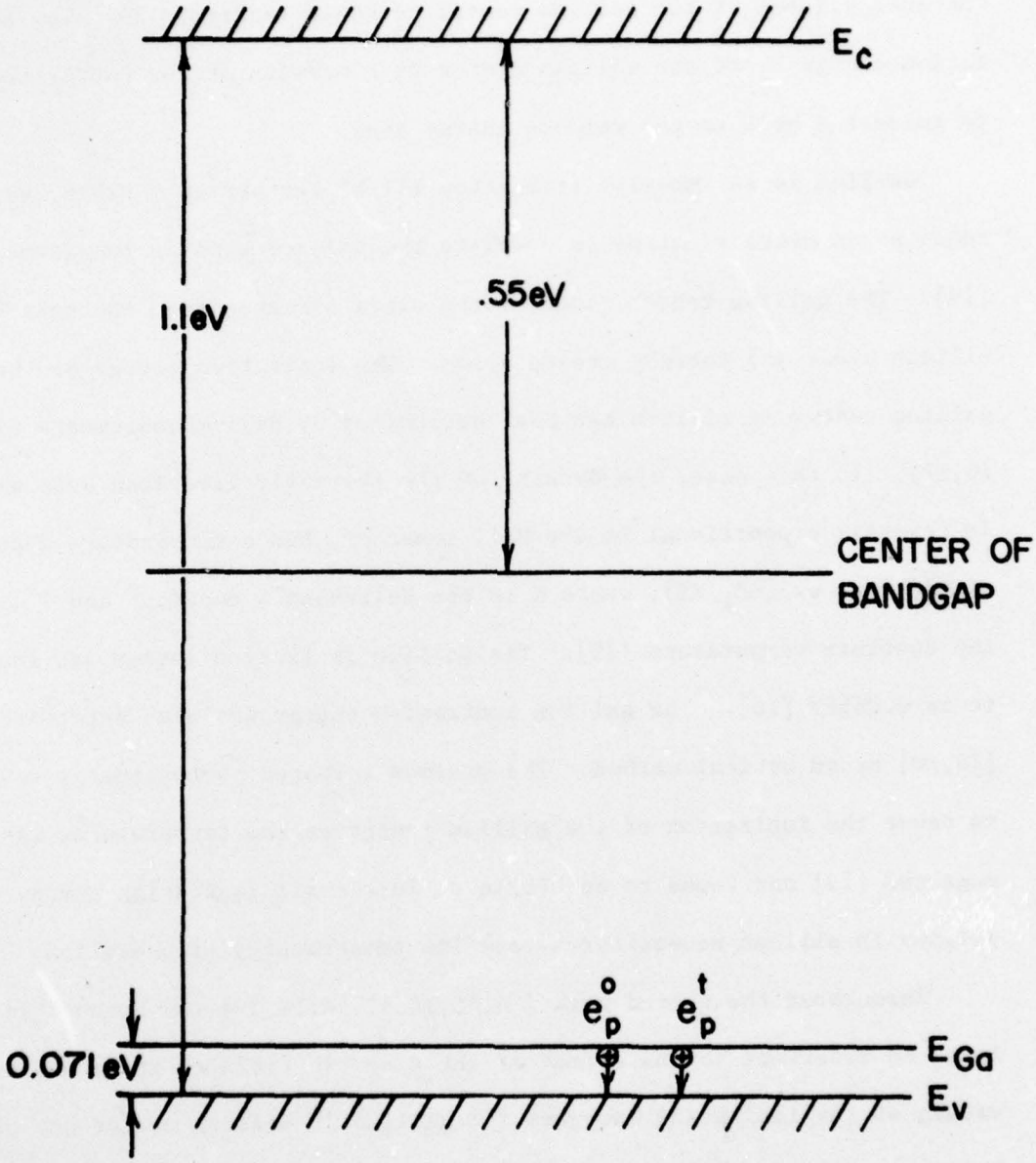

Figure 20 Energy Level of Gallium Center in Silicon at T = 300°K.

The author will attempt to relate the above quoted E_i values to values we measured in his discussion of the Poole Frenkel effect in Section V-A.

The gallium center in silicon at low temperatures, has two distinctly different charge states. The most positive charge state corresponds to the neutral center. i.e. the center when occupied by a hole. The most negative charge state corresponds to the ionized center i.e. the center after emitting a hole to the silicon valence band.

The ionization of the gallium center can be either due to thermal excitation, or to incident photons with energies that correspond to the far infrared radiation wavelength range. The effect of the two charge states of the gallium centers on the operation of the double doped gallium boron MOSFET can only be observed at temperatures below 50°K. The basic physical phenomena determining the operation of the IRFET can be described by the equations of the Shockley-Read-Hall model. It is used for analyzing the effect of the two charge states of the gallium centers in the depletion region on the threshold voltage and channel conductance of the MOSFET.

The gallium doped N-channel MOSFET (IRFET) employs gallium photoionization to modulate the conductance of the channel between the source and drain. A schematic diagram of a cross section in the gallium doped MOSFET is shown on Figure 21. The temperature of operation will be so selected such that the gallium centers are not ionized.

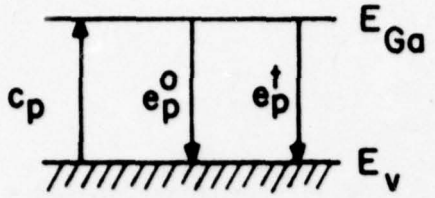

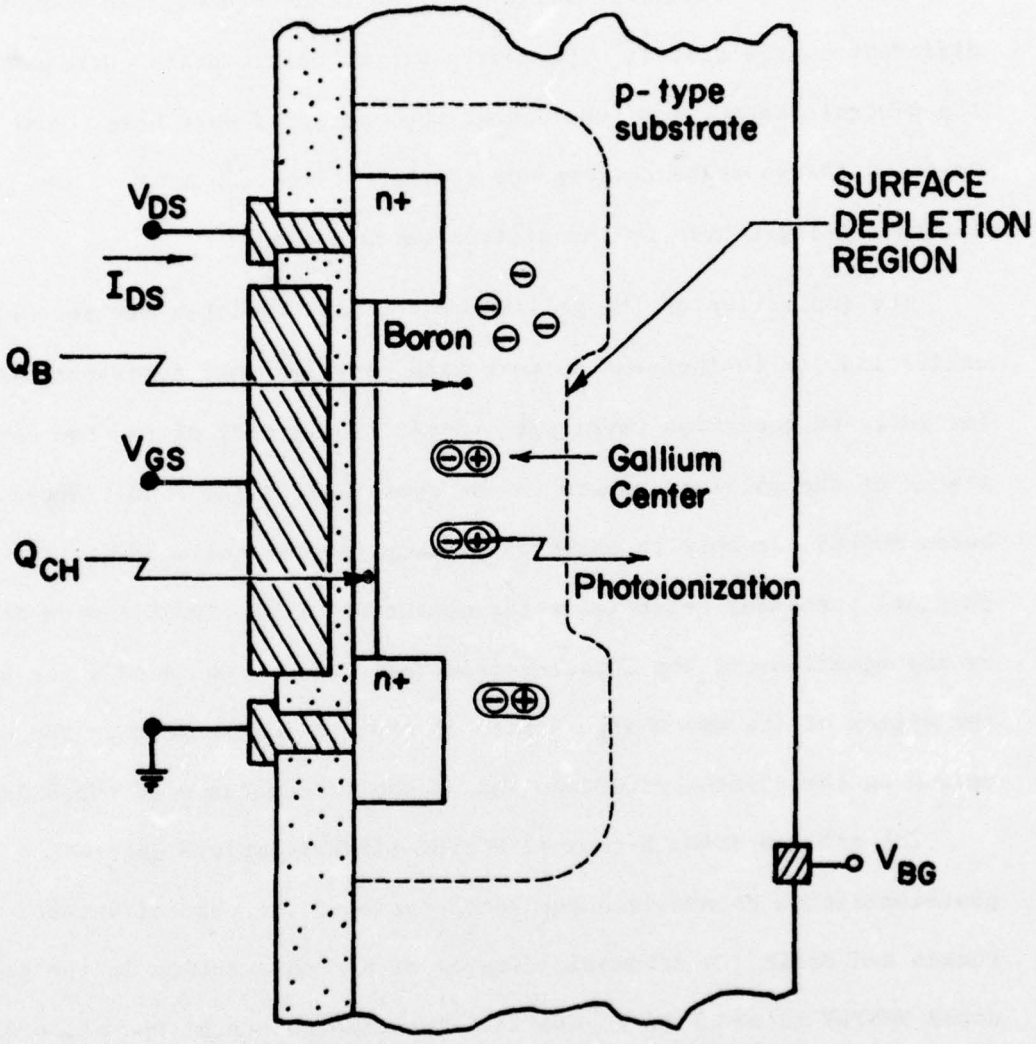

Figure 21 Photoionization of Gallium Centers in the Depletion Region of a MOSFET with Inversion Gate Voltage applied.

When the IRFET is used in an imaging array, it will be turned-on during the period prior to the read out. This period will be referred to in our discussion as the read-in period. If infrared radiation in the 8 to 14 micrometer wavelength range, illuminates the array during the read-in period, the neutral gallium centers in the space charge region will be photoionized by the emission of a hole to the valence band. Consequently, the source to drain resistance of the MOSFET, which is a function of the number of ionized gallium centers in the space charge region, will be modulated by the far infrared radiation. The source to drain resistance of the IRFET is measured during the read-out period, and converted to a digital signal for processing and display.

The gallium doped MOSFET operates consequently as an integrating detector during the read-in period. The gallium centers will be partially or totally ionized at the end of the read-in period and they will remain in the most negative charge state so long that the device is turned on. The read in/out cycle can then be repeated.

The physics of the interaction between the center and the valence band can be interpreted in terms of a hole capture process, C_p, an optical emission process, e_p^o, and a thermal emission process, e_p^t.

The definition of a depletion region, implies the nonexistence of free carriers (holes and electrons). Hence, when the device is on, the mechanism of hole capture for the gallium centers within the depletion region can be ignored. The capture, C_p is important only during the reset operation of the device.

At sufficiently low temperatures, the optical hole emission process from the gallium center to the valence band, e_p^o is dominant. The thermal hole emission rate e_p^t will be effectively eliminated by the proper

selection of the temperature of operation. The time constant (τ), of the gallium ionization in the IRFET will, therefore, be equal to the reciprocal of the optical emission rate, e_p^o.

$$\tau = \frac{1}{e_p^o} \tag{6}$$

A strong field dependence has been observed in the measurements of the thermal emission rate for holes from the gallium centers. A detailed discussion of this observation can be found in Section IV.

The temperature of operation must be selected low enough to allow for gallium deionization. But it must not again be too low, to avoid the deionization of the shallow level acceptor (boron) in the substrate. The ionization energy of boron has been measured [16] and found equal to 0.045 eV. The complete deionization of boron will raise the substrate resistance and may disturb the accuracy of the signal processing.

At the temperature of operation the thermal time constant should be at least two orders of magnitude longer than the read-in/out cycle.

IV. EXPERIMENTAL SET-UP

A. Technique of Measurements

The MOSFET devices were mounted in the sample holder of a cryogenic refrigerator, which is basically a liquid hydrogen cooled cold-finger in an evacuated metal chamber.

A diode sensor mounted on the same cold-finger was used in monitoring the temperature of the device. A radiation shield cooled to 80°K had an aperture facing the filter. The filter was mounted at the same temperature to limit background photon flux.

The experimental set up around the device is shown in Figure 22. The device was triggered by a square wave on the gate. A voltage proportional to the source to drain current was displayed on an oscilloscope. The waveforms were photographed at various thermal, optical and electrical bias conditions. The photocurrent, time constant and other two-charge state characteristics were determined from those photographs. This technique of measurements was necessary due to the fast time constant of gallium ionization at the temperatures of operation.

All voltages were monitored on FLUKE DVM's. The MOSFET and the diode sensor were biased by Hewlett Packard 6216A power supply units. The gate drive voltage was obtained from the bipolar operational power amplifier (KEPCO). The waveforms of the source to drain current were displayed on Tektronix oscilloscope type 561B with a differential amplifier type 2A63.

The MOSFET's used in this experiment had circular structures, with outer, middle and inner rings representing source, gate and drain

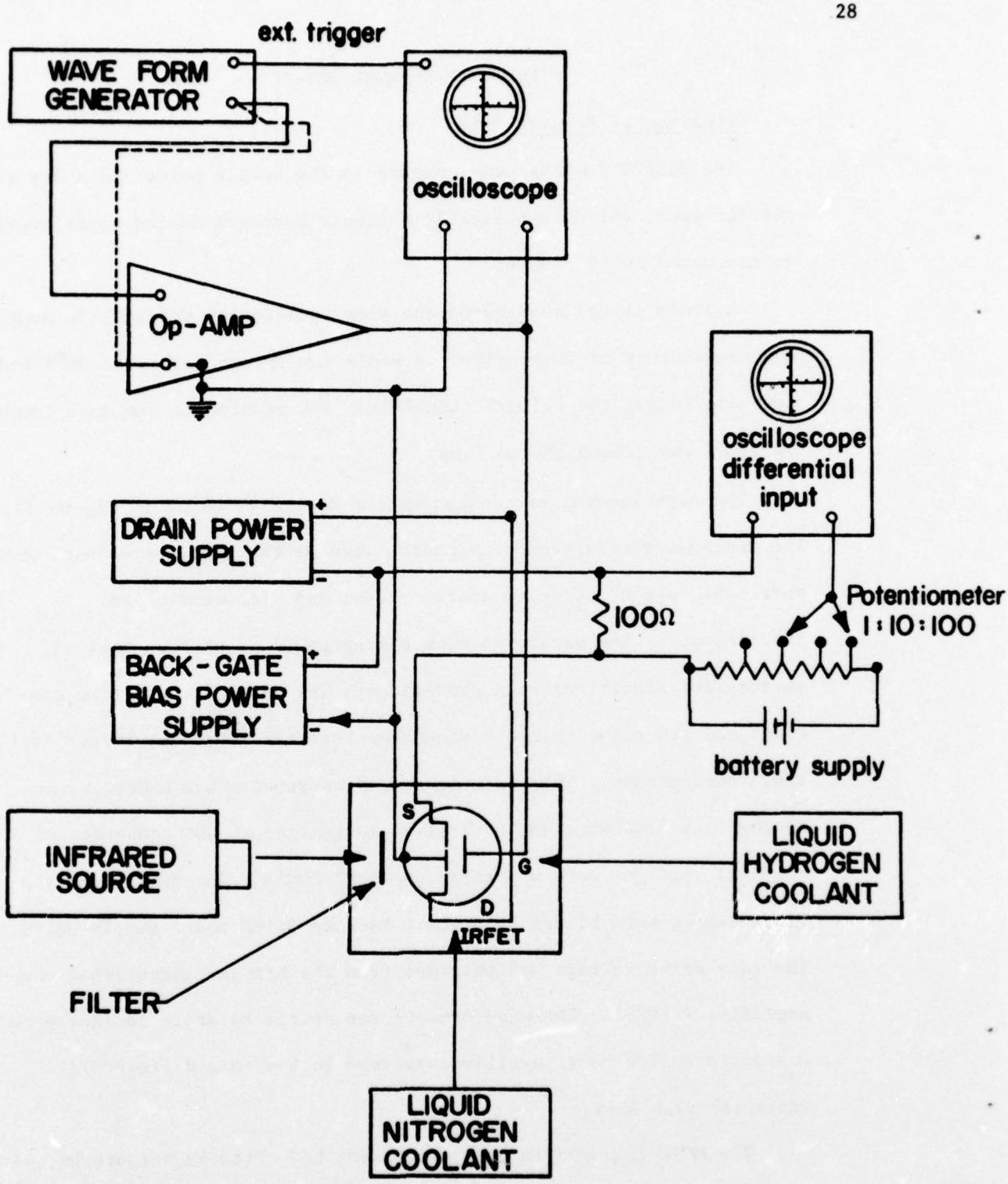

Fig. 22 FLOW CHART OF MEASUREMENT TECHNIQUE

respectively. The dimension of those rings were as follows:

The source outer diameter ≃ 96 miL.

The source inner diameter ≃ 61 miL.

The gate outer diameter ≃ 66.5 miL.

The gate inner diameter ≃ 27.7 miL.

The diameter of the drain circle = 28.5 miL. Therefore $W=\pi(61+28.5)/2$ = 140 MiL, $L=(61-28.5)/2=16.25$ and $W/L \simeq 8.17$

B. Temperature Measurements

A diode sensor was used to measure the temperature of the sample holder in the cryogenic refrigerator. This diode sensor was calibrated in the range between 4.2°K and 100°K. The device was purchased from LAKE SHORE CRYOTRONICS, INC., Model No. DT-500P/GR-I.

The diode was biased in the forward direction by 10 microamperes. A digital voltmeter was used to read the voltage drop across the diode. The measured voltage drop was then converted through the manufacturer's calibration table into temperature readings.

The device had very small mass, dimensions and dissipation in the range of 20 microwatts, to avoid over loading the system thermally. We have neglected in our temperature measurements the error resulting from the limited input impedance of the DVM, in parallel with the diode. We have also assumed that the temperature at the corner of the sample holder, where the diode was mounted, is identical to the temperature of the device. This assumption is practically justified, since the sample holder was designed with minimum dimensions. The diode sensor measured a combination of both the lead and case temperatures. The lead winding around the frame had to be done with extreme care to insure

accurate temperature readings. The manufacturer's calibration table was checked at 77°K and 300°K before the device was used.

Before the diode sensor was purchased, we attempted to measure the temperature by a commercial silicon diode. The same 10 micro-amperes forward bias arrangement was used. Calibration of the voltage drop versus temperature was made at 300°K and 77°K. These two calibration points were used to develop a temperature correction factor. The temperatures were calculated from the ideal I-V diode equation under forward bias condition. This temperature measurement technique, using a commercial diode, left a lot to be desired in terms of accuracy, which ultimately caused us to decide in favor of using the LAKE SHORE diode sensor.

C. Circular Variable Filter [21]

Multilayer coating design allowed the production of any filter in the "CVF" configuration. Optical interference coatings are vacuum deposited on circular germanium substrates. Film thickness, and therefore wavelength, varies linearly with angular position.

The infrared circular variable filter was purchased from OCLI "Optical Coating Laboratory Inc." The infrared range is covered by a set of three 90° segments. The wavelength coverage extends from 2.5 micrometer up to 14.5 micrometer. In the experimental work done on the gallium-boron doped IRFET; only segment three was used. This segment had the following specifications: Wavelength range, λ=7.9 μm to 14.5 μm, half bandwidth < 1.8%, transmittance in band > 30% peak, and blocking for wavelengths below the bandpass; corresponds to a transmission $\leq$ 0.1%. This value is also applicable for wavelengths up to 17.0 μm, when a blocking element is used.

Employing CVF's eliminates the need for multiple filters, and allows for rapid scan capabilities with high resolution. More important, those filters are capable of being operated at cryogenic temperatures, down to $4^{o}K$. The problem of IRFET discharge by photon flux from filters located in $300^{o}K$ ambient, can be eliminated if the filter is attached to the $77^{o}K$ radiation shield. A larger outer chamber for the cryogenic refrigerator had to be designed to accomodate the filter, and allow for segment rotation.

The manufacturer quotes wavelength variations with temperatures of an order less than 1.0% of the center wavelength of the bandpass, per $100^{o}C$. Center wavelength has a tendency to shift to shorter wavelengths with decrease in temperatures [21]. The magnitude of the wavelength shift is dependent on the variation in the refractive indices of the material used as a result of temperature variation. The manufacturer also guarantees the linearity of the transmittance band vs. angle, within 3% range for points at the same radius.

D. Cryogenic Refrigerator

Model AC-2 CRYO-TIP refrigerator was used to carry out the low temperature measurements on the Ga-B doped MOSFET. The system is made by Air products and Chemicals Inc. Model AC-2 is a minuature open cycle Joule-Thomson refrigerator with coil finned heat exchanger. The net refrigeration capacity is 4 watts maximum at $23^{o}K$ [22], the specified temperature range is $16^{o}K$ to $300^{o}K$, and the refrigeration is achieved from standard compressed cylinder gasses (Nitrogen and Hydrogen).

The cooldown time was 45 minutes on the average. The minimum temperature achieved with the WMX-1A vacuum shroud and radiation shield was $21^{o}K$. The radiation shield is kept at approximately the liquid nitrogen

temperature [23], thus providing a shield at about 80°K to the liquid hydrogen (20.4°K) cooled sample holder. The maximum refrigeration capacity is achieved with this configuration, and any increase in the size or mass of the vacuum shroud, radiation shield or specimen holder is bound to increase the lowest achievable temperature [24].

The optical measurements on the Ga-B doped MOSFET had to be conducted with a cold filter. A larger vacuum shroud was designed and produced in the U of A workshop, to enable us to mount and move the circular variable filter in the 80°K temperature station. The operation experience with the AC-2 Cryo-Tip and the heat exchanger model No. AC-2-110, showed that the running time per 220 Cu. ft. N_2 cylinder is 2 hours including the initial load of cooldown. The running time per 220 cu. ft. H_2 cylinder is 3 hours. The N_2 and H_2 cylinders were charged to 2400 PSI and 2100 PSI respectively.

The specimen holders were designed with minimum dimensions, to reduce the thermal load on the cold finger and to obtain the minimum possible coldfinger temperature. The specimen holders were fabricated from copper and oxygen free copper materials due to their good thermal conductivity at low temperatures. Vacuum of $4X10^{-5}$ torr is necessary to limit heat leak, and obtain the lowest operation temperatures.

V. RESULTS AND ANALYSIS

A. Thermal Emission Rate and Poole-Frenkle Effect

To fully characterize the device, one should determine the range of temperatures where the ionization of the gallium center does not occur instantaneously.

The device was triggered by a square wave on the gate with $V_{GS} = \pm 40V$, $V_{BG} = 0$ and $V_{DS} = +10$ volts. A voltage proportional to the source to drain current was displayed on the oscilloscope. The decay of source to drain current, with a time constant, from the initial value to its final value was photographed at various temperatures. The device was fully screened from any radiation source during this process.

The magnitude of the decay in the source to drain current, corresponds to the limit value of the photocurrent, ΔI_{DS} [3]. We have associated the current decay rate with an exponential function and the time constant was determined for each temperature and plotted in Figure 23 versus 1000/T.

Since the thermal emission process is the only ionization process producing this decay, we concluded that the time constant is equal to the thermal time constant and the reciprocal of the thermal emission rate.

$$\tau_t = \frac{1}{e_p^t} \tag{7}$$

In reality, the decay corresponded more to a combination of a fast exponential function superimposed on a slower exponential function, particularly at very low temperatures. The time constants of both of them were temperature dependent, with the fast time constant virtually disappearing at higher temperatures.

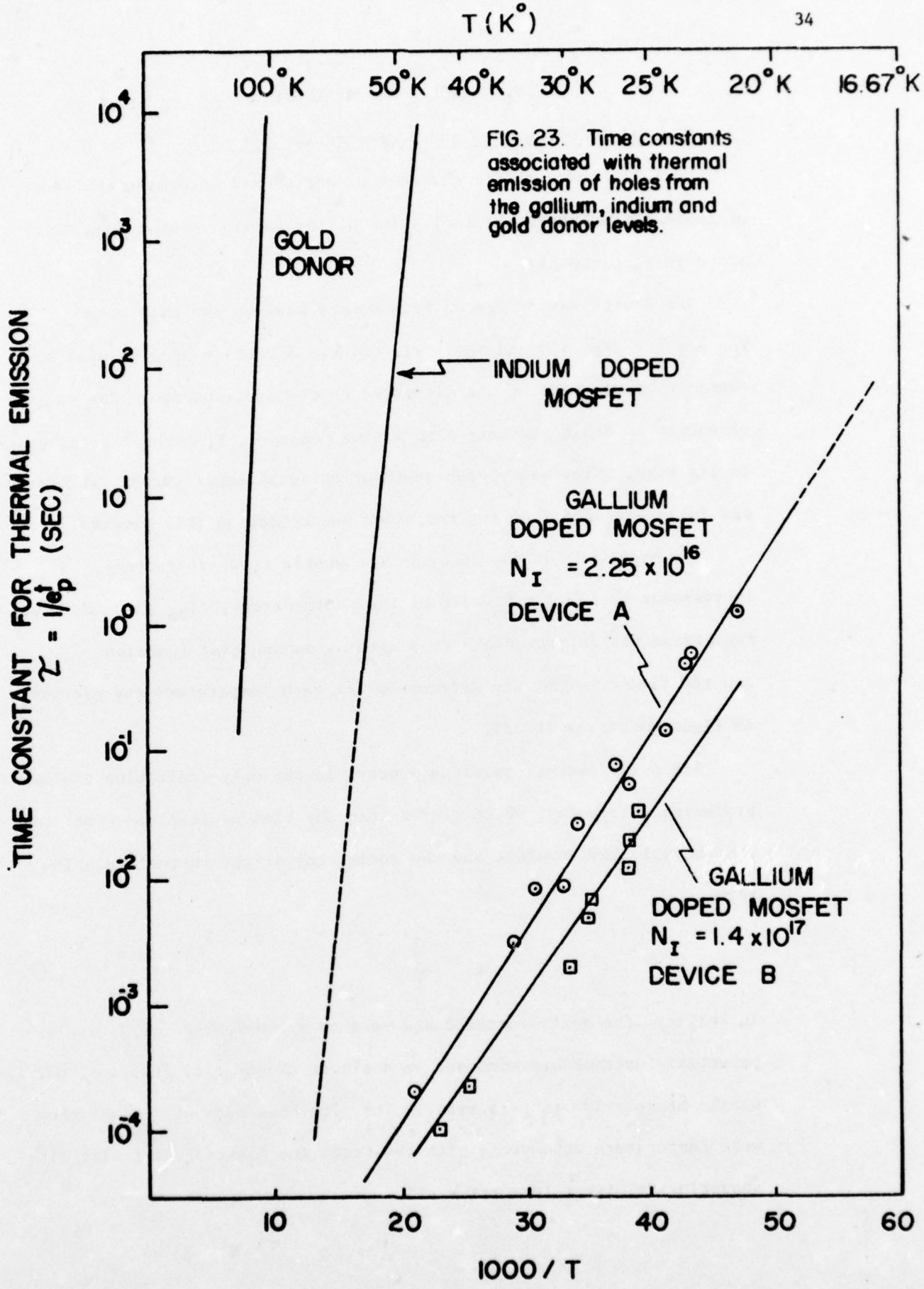

FIG. 23. Time constants associated with thermal emission of holes from the gallium, indium and gold donor levels.

The fast time constant was interpreted as being associated with centers which are physically near to the drain region. Where as the slower time constant is for the gallium centers in the rest of the depletion region. However, this interpretation does not exclude the possibility that some of the fast decay might have been partly due to boron deionization or other causes.

The thermal time constant can be described by the following equation.

$$\tau_t = \frac{1}{e_p^t} = A\, e^{+\Delta E/KT} \tag{8}$$

where ΔE is the activation energy for the center, K is the Boltzmann constant and T is the temperature in ^{o}K. From Figure 23 , A and ΔE can be determined.

For the lightly doped device (A): $N_I = 2.25 \times 10^{16}\ cm^{-3}$

at $\frac{1000}{T} = 33$ $\qquad \tau_t = 10^{-2}$ sec.

at $\frac{1000}{T} = 46$ $\qquad \tau_t = 1$ second

therefore $\tau_t = 1 = A \exp \frac{\Delta E}{K} \frac{46}{1000}$ (9)

$10^{-2} = A \exp \frac{\Delta E}{K} \frac{33}{1000}$ (10)

hence by simple division, we get

$$100 = \exp \frac{\Delta E}{K} \frac{13}{1000} \tag{11}$$

or

$$4.61 = \frac{\Delta E}{K} \frac{13}{1000} \tag{12}$$

therefore

$$\Delta E = 0.0307 \text{ eV} \tag{13}$$

and

$$A = \exp\left(-354.24 \left(\frac{46}{1000}\right)\right)$$

$$= 8.4 \times 10^{-8} \text{ seconds} \tag{14}$$

which is the limit value of the time constant at very high temperatures.

Similarly for the heavily doped device (B): $N_I = 1.4 \times 10^{17} cm^{-3}$

$$\text{at } \frac{1000}{T} = 29 \qquad \tau_t = 10^{-3} \text{sec}$$

$$\text{at } \frac{1000}{T} = 43.4 \qquad \tau_t = 10^{-1} \text{ sec.}$$

therefore

$$\tau_t = 10^{-1} = A \exp \left(\frac{\Delta E}{K} \frac{43.4}{1000}\right) \tag{15}$$

$$10^{-3} = A \exp \left(\frac{\Delta E}{K} \frac{29}{1000}\right) \tag{16}$$

and by simple division, we get

$$100 = \exp \left(\frac{\Delta E}{K} \frac{14.4}{1000}\right) \tag{17}$$

or

$$4.61 = \frac{\Delta E}{K} \frac{14.4}{1000} \tag{18}$$

Therefore

$$\Delta E = 0.02772 \text{ eV} \tag{19}$$

and

$$A = 9.38 \times 10^{-8} \text{ seconds} \tag{20}$$

which is the limit value of the time constant at very high temperatures.

The thermal time constant was found to be strongly field dependent. The decay was several times faster with a very small back gate bias potential applied.

The ionization energy of gallium was measured by others and found equal to 0.071 eV.

In the cases of double doped MOSFET employing gold or indium as second dopant [2], [5], the activation energy determined by the thermal time constant and the temperature; was found to be almost identical with the ionization energies of gold and indium 0.35 eV and 0.155 eV

respectively. However, the deviation observed here, in the case of the gallium center is explainable by the Poole-Frenkel effect. In other words 0.072 eV - 0.0307 eV = 0.0413 eV or 57.4% out of the total ionization energy of the center was supplied by the electric field across the depletion region, rather than by the thermal energy. Simply, since the gallium center is a shallower acceptor, it is more sensitive to the electric field contribution during the ionization. The measurements were repeated with different source to drain voltage V_{DS} and consistent results were obtained.

The rate of hole emission will not only be dependent on the location of the impurity energy level w.r.t. the valence band, but also on the density of unoccuppied states within the valence band [10]. Therefore, we have attempted to match the thermal responce data of Fig. 23, to the following equation:

$$\tau_t = \frac{1}{e_p^t} = A\, T^{-3/2} \exp\,(+\Delta E)/kT. \tag{21}$$

This equation should be valid under the assumption of constant thermal velocity in the temperature range under investigation by ignoring the carrier "heating" resulting from high electric field.

$$(v_{th} = \sqrt{3KT/m} = 3.65X10^{6}\,cm/sec \quad (at\ 29.4^{o}K) \tag{22}$$

at $29.4^{o}K$).

For the lightly doped device (A): $N_I = 2.25X10^{16}cm^{-3}$ we obtain:

$$\Delta E = 0.02725eV \tag{23}$$

and

$$A = 4.94X10^{-5}\ sec.\ {}^{o}K^{-3/2} \tag{24}$$

Similarly for the heavily doped device

$$(B): \quad N_I = 1.4X10^{17}cm^{-3}$$

we obtain:

$$\Delta E = 0.023946eV \tag{25}$$

$$A = 6.47X10^{-5}sec.{}^{o}K^{-3/2}$$

In the following section the field dependance of the emission coefficient for carriers from shallow acceptor levels in the depletion region of Si-MOSFET behind a strongly inverted surface will be derived.

The time dependance of the gallium charge state in the depletion region of the IRFET, can be determined from the Shockley-Read-Hall (SRH) model. The total doping concentration will be defined as

$$N_{TT} = N_A + N_{Ga} \tag{26}$$

in the steady state inversion condition. Where N_A is the concentration of the boron atoms, and N_{Ga} is the concentration of the gallium atoms. In the transient condition that follows the application of an inversion voltage to the gate plate.

$$N_{TT} = N_T + P_T \tag{27}$$

where N_T is the concentration of the negative or ionized acceptor centers, and P_T is the concentration of the centers in the neutral charge state.

W. Shockley and W. T. Read, Jr. have studied the statistics of the recombination occurring through the mechanism of trapping [25], for both equilibrium and nonequilibrium steady state conditions. They also analyzed the rate of generation in the space charge regions. C. T. Sah [26] derived the equivalent circuit model for the SRH center. The equivalent circuit

mentioned above is a powerful tool in determining the response under transient conditions superimposed on an arbitrary steady state force. The rate equations of the above model are now applied to the transient response of the shallow acceptor-gallium center in the depletion region of a double doped gallium-boron MOSFET, which operates at a specific low temperature region which would allow the gallium to be neutral while maintaining total boron ionization. The rate equation describing the change in N_T with respect to time [25, 26] is given by

$$\frac{dN_T}{dt} = C_n n P_T - C_p p N_T + e_p P_T - e_n N_T \tag{28}$$

where e_n is the emission rate of electrons, e_p is the emission rate of holes, C_n is the capture rate of electrons, C_p is the capture rate of holes, n is the number of available electrons and p is the number of available holes. In a depletion region, though, there are no free carriers available for capture, i.e. $n = p = 0$. Thus the rate equation becomes

$$\frac{dN_T}{dt} = e_p P_T - e_n N_T \tag{29}$$

Our initial conditions correspond to the end of the accumulation period at time t=0. During this accumulation period each gallium center captures a hole. Thus, all the gallium centers enter the transient period in their neutral charge state (most positive charge state), where as all the boron centers are ionized (negative charge state). Therefore at t=0

$$N_T(0) = N_A \tag{30}$$

$$P_T(0) = N_{Ga} \tag{31}$$

The final steady state condition with an inverted surface should be

$$N_T(\text{final}) \simeq N_A + N_{Ga} \tag{32}$$

$$P_T(\text{final}) \simeq 0 \tag{33}$$

From equation (27) and (29); we obtain

$$\frac{dN_T}{dt} = e_p(N_{TT} - N_T) - e_n N_T \tag{34}$$

therefore

$$\frac{dN_T}{dt} = e_p N_{TT} - (e_n + e_p)\, N_T \tag{35}$$

from equation (35), we obtain

$$\frac{dN_T}{e_p N_{TT} - N_T(e_p + e_n)} = dt \tag{36}$$

and

$$\frac{dN_T}{N_T - \frac{e_p}{e_p + e_n} N_{TT}} = -(e_n + e_p)dt \tag{37}$$

therefore

$$N_T - \frac{e_p}{e_p + e_n} N_{TT} = C \exp\left(-(e_p + e_n)t\right) \tag{38}$$

where C is a constant.

Equation (38) can also be written in the following form.

$$N_T(t) = C \exp - t/\tau + \frac{e_p}{e_p + e_n} N_{TT} \tag{39}$$

where

$$\tau = \frac{1}{e_p + e_n} \tag{40}$$

We evaluate the constant C from the initial conditions: at $t=0$ $N_T = N_A$

therefore

$$N_A = C + \frac{e_p}{e_p + e_n} N_{TT} \tag{41}$$

and hence

$$C = N_A \frac{e_p}{e_p + e_n} N_{TT}$$

$$= N_A - \frac{e_p}{e_p + e_n} (N_A + N_{Ga})$$

$$C = N_A\left(1 - \frac{e_p}{e_p+e_n}\right) - N_{Ga}\,\frac{e_p}{e_p+e_n} \tag{42}$$

Therefore equation (39) can be written as follows

$$N_T(t) = \left[N_A\,\frac{e_n}{e_p+e_n} - N_{Ga}\,\frac{e_p}{e_p+e_n}\right] \exp -t/\tau + \frac{e_p}{e_p+e_n}\,(N_A + N_{Ga}) \tag{43}$$

In the final steady state condition

$$N_T(\text{final}) = \frac{e_p}{e_p+e_n}\,(N_A + N_{Ga}) \tag{44}$$

But since the gallium acceptor level is much closer to the valence band than to the conduction band, then $e_p >> e_n$ and equations (43) and (44) yield the following two equations:

$$N_T(t) \simeq - N_{Ga}\, e^{-t/\tau} + N_A + N_{Ga} \tag{45}$$

$$N_T(\text{final}) \simeq N_A + N_{Ga} \tag{46}$$

where the average time constant $\tau = \frac{1}{e_p}$ under nonequilibrium conditions. e_p is comprised of both the thermal field assisted emission rate $e_p^{t,\varepsilon}$ and the optical emission rate e_p^o, therefore

$$e_p = \frac{1}{\tau} = e_p^{t,\varepsilon} + e_p^o \qquad (1/\text{sec}) \tag{47}$$

substituting for both the thermal field assisted emission rate $e_p^{t,\varepsilon}$ and the optical emission rate in equation (47) yields the equation of the general emission rate of an electric field tunnable infrared detector.

$$e_p = A\, e^{-\Delta E_t/KT} + B\, e^{+\beta E^n/nT} + \sigma_p^o\,\Phi \tag{48}$$

where A,B have the dimensions of $\frac{1}{\text{sec}}$

A + B : is the emission rate at low electric field and high temperature while the device is operating in the dark

σ_p^o : is the photoionization cross section (cm^2)

Φ : photon flux #/cm^2 . sec

ΔE_t : the thermal activation energy

E : the average or mean electric field

n : a constant. The value of this constant depends on the degree of nonlinearity of the electric field in the depletion region of the MOSFET.

β : the Poole-Frenkel constant

$$\beta = (q^3/\pi K_{si}\varepsilon_o)^{\frac{1}{2}} \tag{49}$$

K : the Boltzmann constant

T : the temperature in ^oK

As shown earlier; we measured the response of the gallium center in the depletion region of a MOSFET behind a strongly inverted surface. If the thermal activation energy ΔE_t determined from these measurements were added to the barrier lowering due to electric field, the result would be related to the ionization energy of the gallium center, [16, 19].

The Poole-Frenkel theory predicts that the electric field will lower the coulomb barrier by an amount proportional to $E^{\frac{1}{2}}$, thus increasing the probability of thermally induced-emission [8]. By applying a simple one dimensional Poole-Frenkel model we will illustrate how the probability of thermally induced emission is enhanced by electric field. The Poole-Frenkel effect is very similar to the field assisted Schottky emission [8,9], but it is twice as strong because the interaction of the escaping carrier is with a fixed point charge rather than with an image charge [8].

Since the maximum electric field across the depletion region in both device A and B is less than 6×10^5 V/cm, we do not expect that ionization by carrier tunneling has played any significant role in the device operation. However, the thermal velocity can be much larger [8] than that corresponding to the lattice temperature because of carrier "heating" by electric field

larger than 100 V/cm at temperatures below 77°K [8].

In a n-channel MOSFET the band bending at the surface when the device is on developes the surface potential, ϕ_s. The surface potential is approximately equal to

$$\phi_s \simeq 2\phi_f + V_{BG} \tag{50}$$

under back gate bias condition. The surface potential however, is also effected by the drain to source voltage. If the later results in a uniform spatial electric field across the surface, then we can approximate the surface potential as follows:

$$\phi_s \simeq 2\phi_f + V_{BG} + \frac{V_{DS}}{2} \tag{51}$$

at a point midway between the source and drain. This approximation does not take in account the effect of channel pinch off on the linearity of the voltage distribution along the channel.

The maximum depletion layer depth, as defined in the MOS theory [27], would be equal to

$$X_D = \sqrt{\frac{2\kappa_{si}\varepsilon_o\phi_s}{qN_T(t)}} \tag{52}$$

where ϕ_s is the surface potential as defined by either equation(50) or (51), $N_T(t)$ is the concentration of the ionized acceptors as defined by either equation (43) or (45), $\kappa_{si} = 12$, $\varepsilon_o = 8.85 \times 10^{-4}$ F/cm and q is the electronic charge $\simeq 1.6 \times 10^{-19}$ coulomb. We conclude from equation (52) that the depth of the depletion layer is a function of time during the transient period or the read-in period. The maximum depletion layer depth occurs when $N_T(t) = N_A$, and the minimum occurs at the end of the gallium ionization process when $N_T(t) = N_A + N_{Ga}$. If the effect of space charge on the voltage distribution across the depletion layer is ignored, in other words, if we assume that the voltage drop is linearly distributed in the direction normal to the silicon surface, then the electric field is constant along the depletion layer depth and equals

$$E = \frac{\phi_s}{X_D} \tag{53}$$

We conclude from equation (53) that the electric field across the depletion layer is also a function of time as a result of the time varying depletion layer depth. This ultimately means that the emission rate as defined in equation (48) is also a function of time through its exponential dependance on the electric field, with the minimum emission rate occurring at the beginning of the ionization process and the maximum emission rate occuring at the end of that process. This can also explain why did the decay time constant appear as an initial fast decay superimposed on a slower decay.

From equation (45) we will calculate now the mean doping in the depletion region during the transient under the assumption that $e_p >> e_n$.

$$\langle N_T \rangle = \int_0^{4\tau} \frac{N_T(t)}{4\tau} \, dt = N_A + 0.755\, N_{Ga} \tag{54}$$

$$\langle X_D \rangle = \sqrt{\frac{2\kappa_{si}\varepsilon_o\phi_s}{q(N_A + 0.755\, N_{Ga})}} \tag{55}$$

$$\langle E \rangle = \frac{\phi_s}{\langle X_D \rangle} \tag{56}$$

Now, for device A, at low temperature, under the assumption that the fermi level lies above the boron energy level and below the gallium energy level in the bulk silicon such that all the gallium atoms are neutral except when the device is turned on.

$$\langle N_T \rangle = 1.8 \times 10^{16} + 0.755\ (0.45 \times 10^{16})$$
$$= 2.1 \times 10^{16}\ /cm^3 \tag{57}$$

and using the surface potential approximation of equations (50) and (51) we calculate the mean depletion layer depth where $2\phi_f \simeq 1$ at low temperatures From equation (50)and (55) we obtain

$$\langle X_D \rangle = \sqrt{\frac{2 \times 12 \times 8.85 \times 10^{-14}(1 + V_{BG})}{1.6 \times 10^{-19} \times 2.1 \times 10^{16}}}$$

$$\simeq 2.5 \times 10^{-5} (1 + V_{BG})^{1/2} \quad (58)$$

where as from equation (51) and (55) we obtain

$$\langle X_D \rangle \simeq 2.5 \times 10^{-5} \left(1 + V_{BG} + \frac{V_{DS}}{2}\right)^{1/2} \quad (59)$$

from the equations (56) and (58), we deduce that

$$\langle E \rangle \simeq 3.98 \times 10^{4} (1 + V_{BG})^{1/2} \quad (60)$$

and from the equations (56) and (59), we obtain

$$\langle E \rangle \simeq 3,98 \times 10^{4} \left(1 + V_{BG} + \frac{V_{DS}}{2}\right)^{1/2} \quad (61)$$

Now let us calculate the Poole-Frenkel constant β:

$$\beta = \left(\frac{q^3}{\pi K_{si} \varepsilon_o}\right)$$

$$= \left(\frac{1.6 \times 10^{-19}}{3.14 \times 12 \times 8.85 \times 10^{-14}}\right)^{1/2} \simeq 2.2 \times 10^{-4} \ eV\left(\frac{cm}{V}\right)^{1/2} \quad (62)$$

$$KT \text{ at } 26^{o}K = \frac{1.38 \times 10^{-23}}{1.6 \times 10^{-19}} \ 26 = 2.24 \times 10^{-3} eV \quad (63)$$

$$KT \text{ at } 34.7^{o}K = 8.617 \times 10^{-5}(34.7^{o}) = 2.99 \times 10^{-3} eV \quad (64)$$

from (62) and (63)

$$\frac{\beta}{KT}\Big]_{\text{at } 26^{o}K} = \frac{2.2 \times 10^{-4}}{2.24 \times 10^{-3}} = 9.82 \times 10^{-2} \quad (65)$$

from (62) and (64)

$$\frac{\beta}{KT}\Big]_{\text{at } 34.7^{o}K} = \frac{2.2 \times 10^{-4}}{2.99 \times 10^{-3}} = 7.36 \times 10^{-2} \quad (66)$$

Therefore using equation (60) and both equations (65) and (66), we conclude that the rate of hole emission is proportional to the following

$$e_p \propto \exp \frac{\beta}{KT} E^{\frac{1}{2}} \tag{67}$$

assuming a constant electric field across the depletion layer.

At $26^{\circ}K$ for device A we get

$$e_p \propto \exp 9.82 \times 10^{-2} \times 199.5 \, (1 + V_{BG})^{\frac{1}{4}} \tag{68}$$
$$\propto \exp 19.6 \, (1 + V_{BG})^{\frac{1}{4}}$$

At $34.7^{\circ}K$ for device A we get

$$e_p \propto \exp 14.6 \, (1 + V_{BG})^{\frac{1}{4}} \tag{69}$$

Equations (68) and (69) are plotted together with the measured data on Figure 24. The slopes of the resulting lines on a semi-log plot match the measured points very closely.

The barrier lowering, at $(V_{BG} = 0)$, can be calculated from the Poole-Frenkel model

$$\Delta\phi_{PF} = \beta\sqrt{E} = 2.2 \times 10^{-4} \times 199.5 = 0.0439\text{eV}$$

Now summing the barrier lowering with the measured activation energy we get the ionization energy of the gallium center.

$$\varepsilon_i = \Delta E_t + \Delta\phi_{PF}$$
$$= 0.02725 + 0.0439 = 0.071\text{eV} \tag{70}$$

which is identical to the ionization energy of the gallium center measured by E. Burstein in 1955 [19].

Similarly using equation (61) and both equations (65) and (66), we obtain the proportionality between the hole emission rate and the electric field.

At $26^{\circ}K$ for device A we get

$$e_p \propto \exp 19.6 \, (1 + V_{BG} + \frac{V_{DS}}{2})^{\frac{1}{4}} \tag{71}$$

and at $34.7^{\circ}K$ for device A we get

$$e_p \propto \exp 14.6 \, (1 + V_{BG} + \frac{V_{DS}}{2})^{\frac{1}{4}} \tag{72}$$

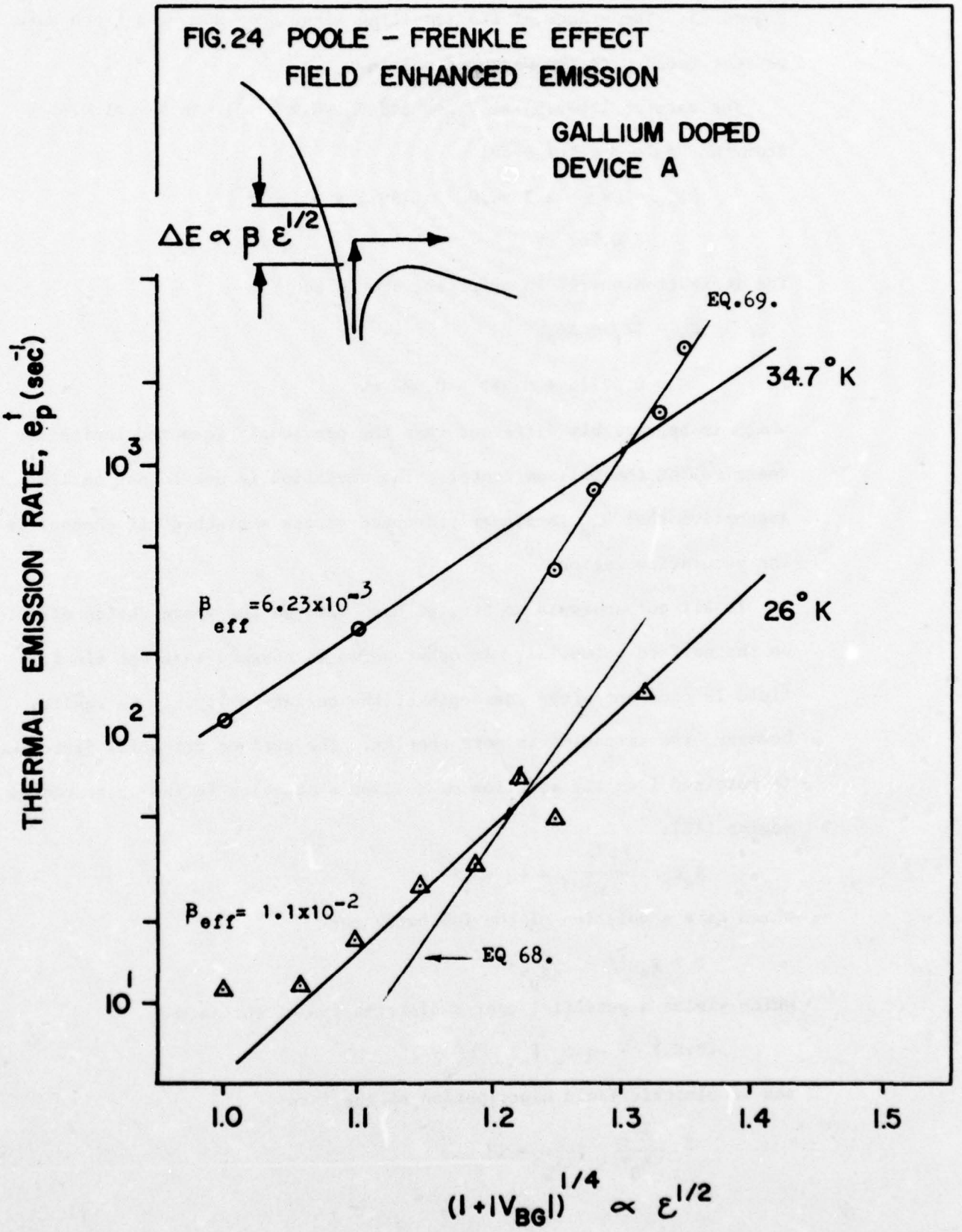
FIG. 24 POOLE - FRENKLE EFFECT
FIELD ENHANCED EMISSION
GALLIUM DOPED
DEVICE A
ΔE ∝ β ε^1/2
EQ.69.
34.7°K
26°K
β_eff=6.23x10^-3
β_eff= 1.1x10^-2
EQ 68.
THERMAL EMISSION RATE, e_p^t (sec^-1)
10^3
10^2
10^1
1.0
1.1
1.2
1.3
1.4
1.5
(1+|V_BG|)^1/4 ∝ ε^1/2

Equations (71) and (72) are plotted together with our measurements on Figure 25. The slopes of the resulting lines on a semi-log graph make perfect match with the measured points.

The barrier lowering at V_{BG}=0 and V_{DS}=8.9 volt, can be calculated from the Poole-Frenkel model

$$\Delta\phi_{PF} = \beta\sqrt{E} = 2.2 \times 10^{-4} \times 199.5 \times (1 + \frac{8.9}{2})^{\frac{1}{4}} = 0.067 \text{ eV} \quad (73)$$

The ionization energy in this case should be

$$\epsilon_i = \Delta E_t + \Delta\phi_{PF} = 0.02725 + 0.067 = 0.094 \text{ eV} \quad (74)$$

which is appreciably different than the previously measured ionization energies for the gallium center. The deviation is due to our earlier assumption that V_{DS} is linearly dropped across a pinched off channel in the saturation region.

In all our analysis so far, we have ignored the space charge effect on the surface potential. In other words we assumed that the electric field is constant along the depth of the depletion layer. In reality however, the situation is more complex. The surface potential distribution is obtained from the solution of Poisson's equation in the space charge region [12].

$$K_s\epsilon_o \frac{\partial^2\phi}{\partial x^2} = -q \langle N_T \rangle \quad (75)$$

which have a solution of the following form

$$\phi = \phi_s \left[1 - \frac{x}{\langle X_D \rangle}\right]^2 \quad (76)$$

which yields a potential energy distribution of the form

$$(P.E.) = -q\,\phi_s \left[1 - \frac{x}{\langle X_D \rangle}\right]^2 \quad (77)$$

and an electric field distribution of the form

$$E = \frac{2\phi_s}{\langle X_D \rangle} \left[\frac{x}{\langle X_D \rangle} - 1\right] \quad (78)$$

FIG. 25 POOLE - FRENKLE EFFECT
FIELD ENHANCED THERMAL EMISSION

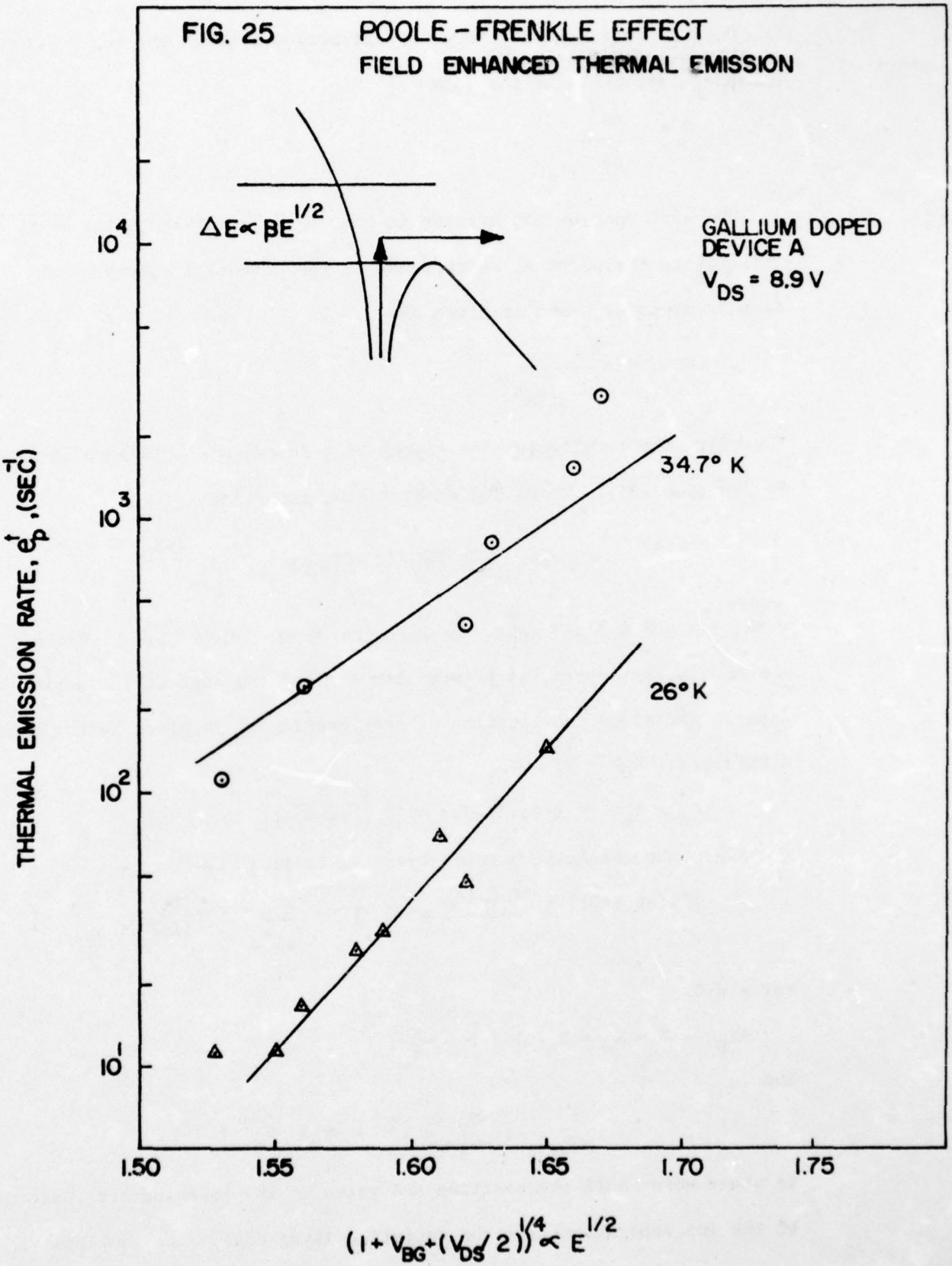

On the other hand the force of attraction between the ion and the escaping carrier is of the form

$$F_a = \frac{-q^2}{4\pi\kappa_{si}\varepsilon_e x^2} \tag{79}$$

The work done by the carrier in the course of its transfer from infinity to the point x, corresponds to the potential energy of the carrier at point x and is given by

$$(PE)c = \frac{q^2}{4\pi\kappa_{si}\varepsilon_o x} \tag{80}$$

Therefore the total potential energy as a function of distance is given by equation (81). Where X=0 at Si - SiO_2 interface.

$$PE(x) = \frac{q^2}{4\pi\kappa_{si}\varepsilon_o[(\langle X_D\rangle - x) - y]} + q\frac{\phi_s}{\langle X_D\rangle^2}(\langle X_D\rangle - x)^2 \tag{81}$$

where:
$y < \langle X_D\rangle - x$ and $0 < x < \langle X_D\rangle$. as illustrated on Fgiure (26-A). Where y Figure 26 is the separation between the ion and the edge of the depletion layer. Therefore the location of the lowering x_m is given by the condition

$d[PE(x)]/d[\langle X_D\rangle - x] = 0$

$$X_D - X'_m = X_m(\text{at } y{-}0) = \left[\frac{1}{[4\pi\langle N_T\rangle]}\right]^{1/3} \text{ cm} \tag{82}$$

therefore the resulting barrier lowering is equal to

$$|\Delta\phi(\text{at } y{=}0)| = \frac{P.E.(X_m)}{q} = \frac{3}{2}\frac{q}{\kappa_{si}\varepsilon_o}\left[\frac{\langle N_T\rangle}{16\pi^2}\right]^{1/3} \text{ volts} \tag{83}$$

for $y \neq 0$

$$\langle X_D\rangle - X = X_m = X_m(0)\left[1 - \frac{y}{X_m}\right]^{-\frac{2}{3}} \tag{84}$$

and

$$\Delta\phi = \frac{q}{2\kappa_{si}\varepsilon_o}\left[\left(\frac{\langle N_T\rangle X_m}{\pi}\right)^{1/2} + \langle N_T\rangle X_m^2\right] \tag{85}$$

In other words both the position and value of the lowering are functions of the ion separation from the depletion layer edge. The complexity

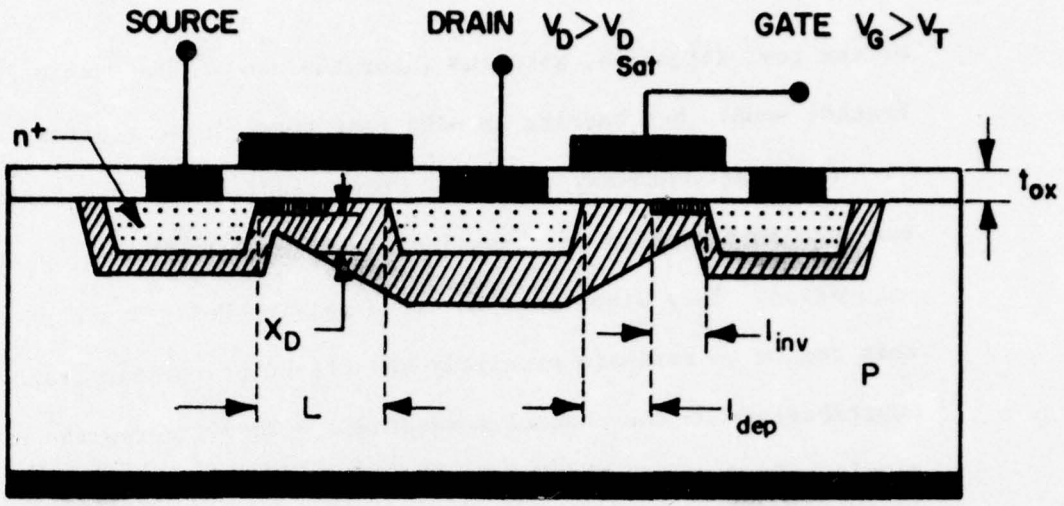

CROSS SECTION OF MOS-
TRANSISTOR OPERATING IN SATURATION

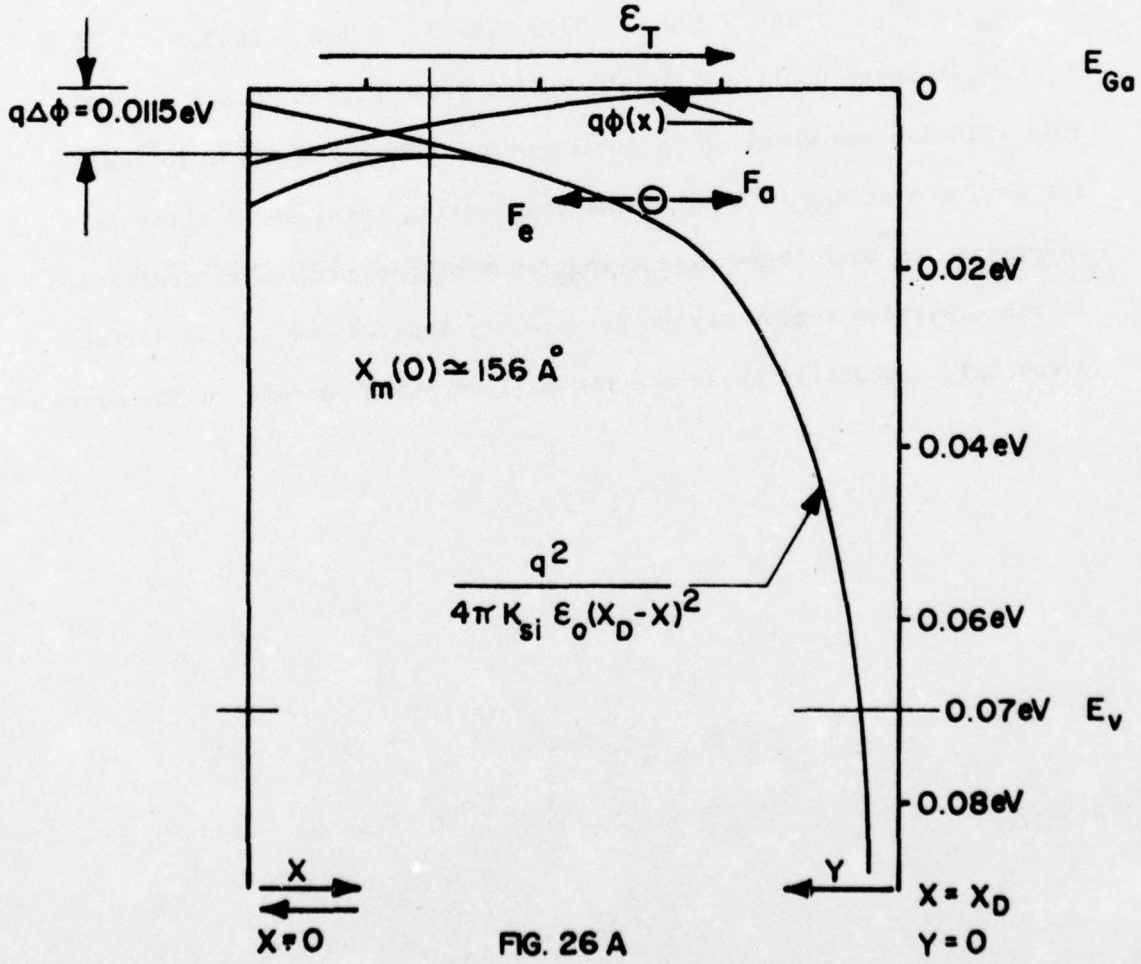

FIG. 26 A

Barrier Lowering by Electric Field .

of the real situation, makes us favor the use of the simple Poole-Frenkel model, but barring in mind that there is some error evolved.

D. F. Bentchkowsky and A. S. Grove studied electric field disturbance in the drain to channel region [28] for a device operating in saturation. They also tried to avoid solving Poisson's equation is this region to estimate precisely the effect of the two transverse field contributions on the channel conductance. They favored the use of a simple less accurate model over the complexity of the solution of Poisson's equation in the channel region.

The solutions of the equations (84) and (85) are summarized in the following table and plotted on figure (26-B).

y in A^o	0	20	40	60	100	2000	2400
x_m in A^o	156	170	183.8	197.8	228.8	2043.1	2439.4
$\Delta\phi_m$ in volts	0.01156	0.0126	0.0137	0.0148	0.0175	0.688	0.972

This solution was obtained by substituting $\langle N_T(t)\rangle = 2.1 \times 10^{16} cm^{-3}$ for device A at $V_{BG} = 0$. The most interesting thing about those calculations, is that they suggest that some of the gallium concentration in the depletion region may be permanently ionized due to the surface potential. Naturally those are the gallium atoms nearest to the surface.

FIG. 26B Graphical Representation of the Solution of Poissans Equation in the Depletion Region of Ga-B doped MOSFET

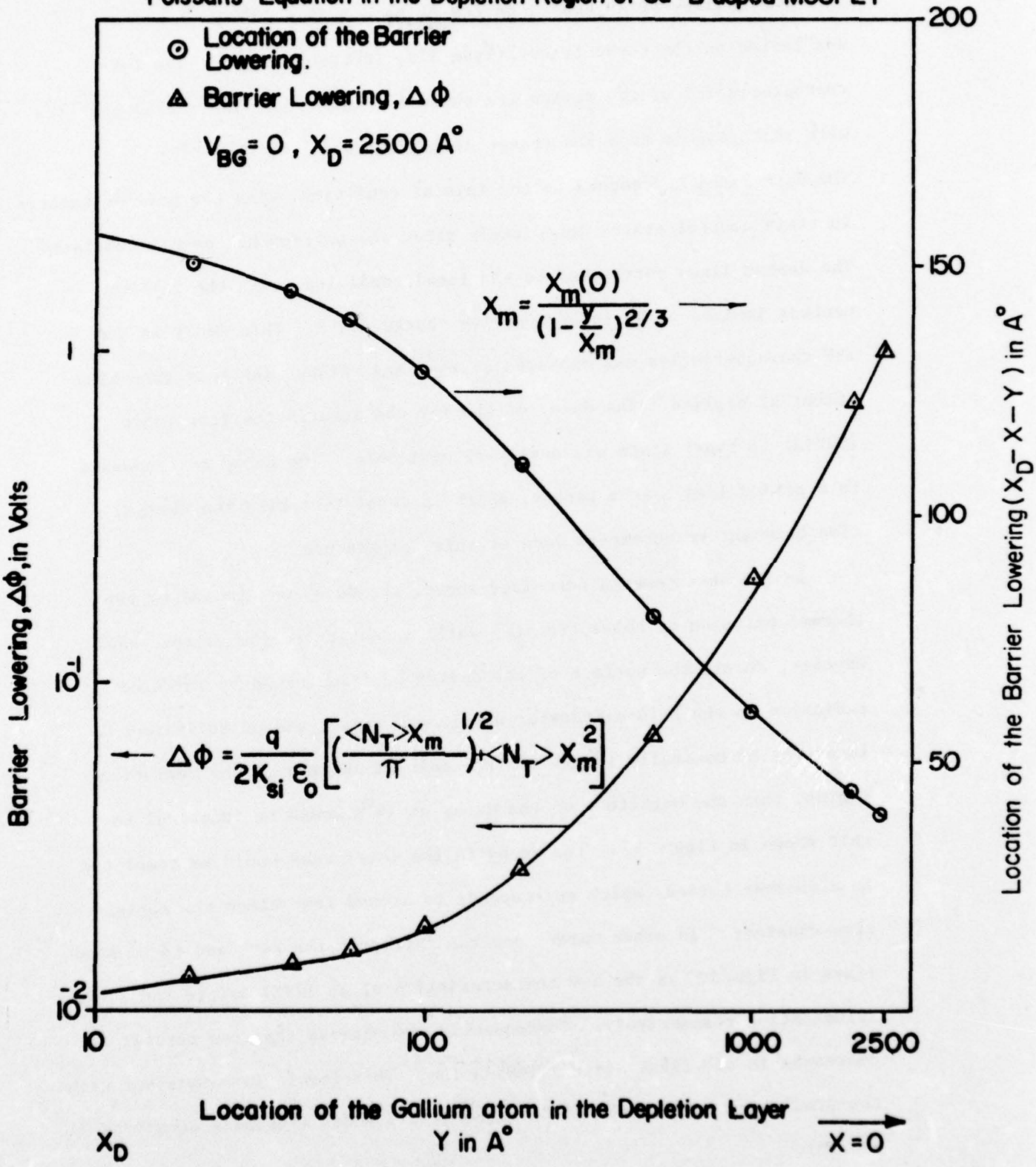

B. Two Charge State Device Characteristics

The gallium-boron MOSFET device A, $N_I = 2.25 \times 10^{16} cm^{-3}$ was tested on the curve tracer (Type 576, Tektronix Inc.). The I-V characteristics of the device are shown in Figure 27 . The characteristics were photographed from the tracer display with a time exposure. The dark lines correspond to the initial condition, with the gallium centers in their neutral state, immediately after the surface has been accumulated. The dashed lines correspond to the final condition, with the gallium centers ionized or in their negative charge state. This decay in the I-V characteristics was measured at $24^{o}K$ and without any back gate bias potential applied. The decay of the I-V characteristics from their initial to final state was easily recognizable. The decay corresponded to a period less than a second, which is consistent with the thermal time constant measurements done at this temperature.

In the measurements described above, the decay was caused by the thermal emission of holes from the gallium centers to the valence band. However, should the surface of the device be illuminated by infrared radiation in the 8-14 micrometer wavelength range; and of sufficient intensity to optically ionize all the gallium centers in the depletion region, then the magnitude of the decay at $24^{o}K$ would be identical to this shown in Figure 27. The decay in the later case would be completed in a shorter period, which corresponds to around four times the optical time constant. In other words, one can interpret the dark and the dashed lines in Figure 27 as the I-V characteristics of an IRFET before and after illumination respectively. Consequently, we observe that the current decreases in the IRFET after illumination. This result is consistent with the prediction made in the IRFET mathematical model (Appendix Equations 24 and 25).

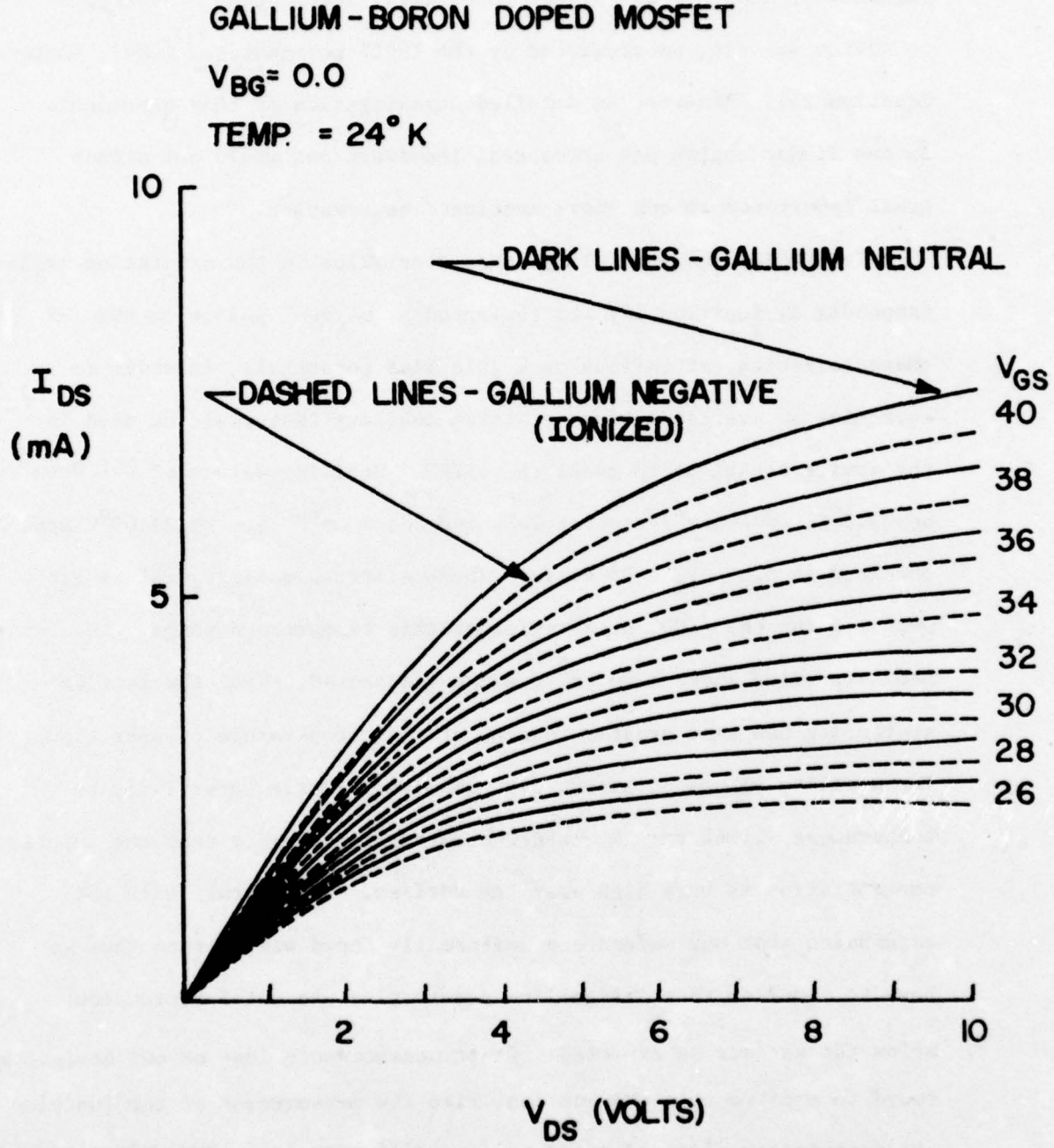

FIG. 27 The I-V characteristic of an IRFET before and after illumination.

The photocurrent ΔI_{DS} is the difference in current at two corresponding points on the dark and dashed lines of Figure 27, at the same electric bias conditions. In the linear region of the I-V characteristics of Figure 27 , ΔI_{DS} did not appear to be fully independent of the gate to source voltage, as predicted by the IRFET mathematical model, (Appendix Equation 24). However, no detailed investigation of this dependence in the linear region was attempted, therefore one would not attach great importance to our above mentioned observation.

The MOSFET current-voltage characteristics in the saturation region, (Appendix A, Equation 22) was evaluated at several points on the I-V characteristics, at various back gate bias potentials, in order to determine an average surface electron mobility that could be used in the device equations to model the IRFET. Mobility values of 257.0 $cm^2/V.sec$ at 29.3°K, 286.4 $cm^2/V.sec$ at 24°K and 286.6 $cm^2/V.sec$ at 23.09°K were obtained at $V_{GS} - V_T \simeq 35$ volts. These electron mobility values are very low for the (100) orientation at this temperature range. An electron mobility value above 1200 $cm^2/V.sec$ was expected, since the lattice scattering has been greatly reduced at this temperature of operation [29]. The mobility values obtained, also show very little sensitivity to temperature -1.66% per °K. These observations suggest that the impurity concentration is very high near the surface. If we start with the assumption that our wafers are uniformally doped with boron; then we have to conclude that the gallium penetration was not 5 micron deep below the surface as expected. Other measurements done on our devices were found to confirm this observation, like the measurement of the junction characteristics obtained after gallium diffusion in P-type wafers and the dependence of ΔV_T on the back gate bias potential.

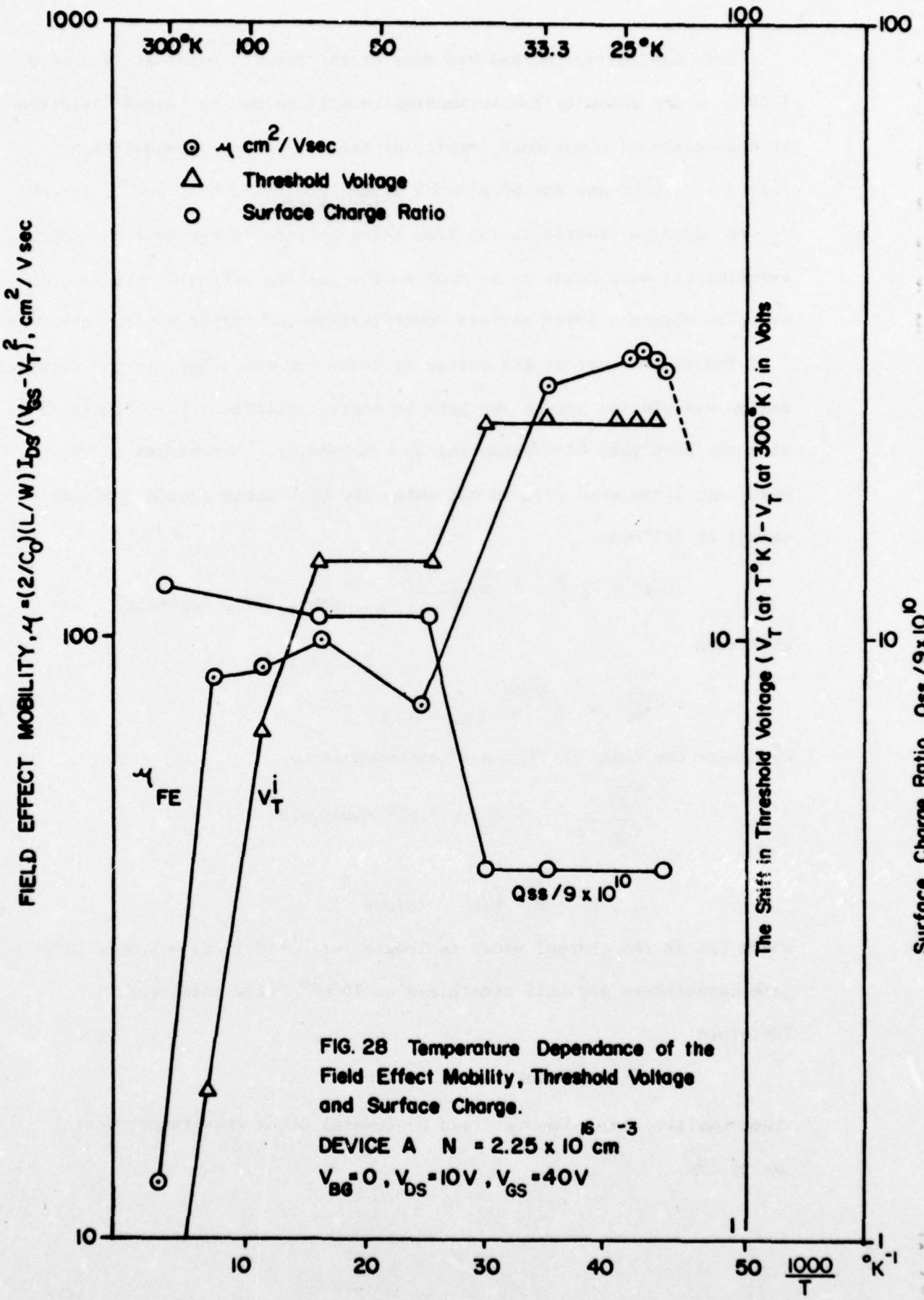

FIG. 28 Temperature Dependance of the Field Effect Mobility, Threshold Voltage and Surface Charge.

DEVICE A $N = 2.25 \times 10^{16}\ cm^{-3}$

$V_{BG} = 0$, $V_{DS} = 10V$, $V_{GS} = 40V$

This conclusion contradicts some of the results obtained by others [10] on the impurity redistribution in silicon due to thermal oxidation. It also makes it clear that inspite of the 30 minutes predeposition period at 1200°C and the 60 minutes drive in diffusion at 1100°c in wet O_2, the gallium profile is far from being uniform in our devices. More experimental work needs to be done on the gallium diffusion process, in order to obtain a lower surface concentration and better surface parameters.

The square root of the source to drain current, $\sqrt{I_{DS}}$, in the saturation region was plotted versus the gate to source potential, V_{GS}, Figure 29 , with the back gate bias potential as a parameter. The slopes of the resulting lines were used to determine the previously quoted mobility values as follows:

$$I_{DS} = \mu C_o \frac{W}{L} \left(\frac{V_{GS} - V_T}{2} \right)^2 \qquad \text{(Eqn, (22), Appendix)}$$

Therefore

$$\sqrt{I_{DS}} = \sqrt{\frac{\mu C_o W}{2L}} (V_{GS} - V_T) \tag{86}$$

Therefore the slope in Figure 29 corresponds to

$$\frac{\sqrt{I_{DS}}}{V_{GS} - V_T} = 2.3 \times 10^{-3} \sqrt{\text{Amp}}/\text{volt}. \tag{87}$$

$$\therefore \mu = \frac{2}{C_o} \frac{1}{W/L} (\text{slope})^2 \tag{88}$$

where W/L is the channel width to length ratio = 8.17 C_o = 5.06×10^3pf = gate capacitance per unit area based on 7000A° oxide thickness.

Therefore

$$\mu = 257.06 \quad \text{Volt/cm}^2\text{.second}. \tag{89}$$

This mobility value was verified by several other measurement sets at 29.4°K.

We calculated the electron mobility from equation (88) as the temperature went down. The mobility peaked around 100°K then dropped slightly in value, then increased to a maximum of around 286 cm^2/Vsec at 23°K. The results of these calculations are plotted on Figure 28. F. Fang and A. Fowler have also measured [29] the effective mobility on the (100) orientation. They kept however, the source to drain voltages low to avoid the hot electron effect and the non-uniformity of the surface field across the sample [29]. They reported that the mobility measured at varying electric field at low temperatures, has increased initially to a 1300 cm^2/Vsec peak at 2 x 10^5 V/cm electric field then dropped rapidly as the electric field was increased further. The samples used in these measurements were characterized by high substrate resistance or very low doping (129 ohm-cm).

The mobility has increased consistently as the temperature went down. The mobility peak (1300 cm^2/Vsec) was obtained at around 30°K, thereafter much less temperature sensitivity was reported. This last set of measurements was carried out on a 1.88 ohm-cm sample, (100) orientation and when the gate voltage was 15 volt above the threshold.

These results are consistent with the general trend that we have observed. The deviation is in the order of magnitude of the surface mobility, as a consequence of the gallium accumulation at the surface. We found also that there is no single power law $\exp\left(\frac{-E}{KT}\right)$ that can explain the mobility-temperature dependence over the entire observation range.

The temperature dependence of the threshold voltage on device A was measured. On Figure 28 we plotted the shift in the threshold voltage from its value at room temperature versus 1000/T. The shift in

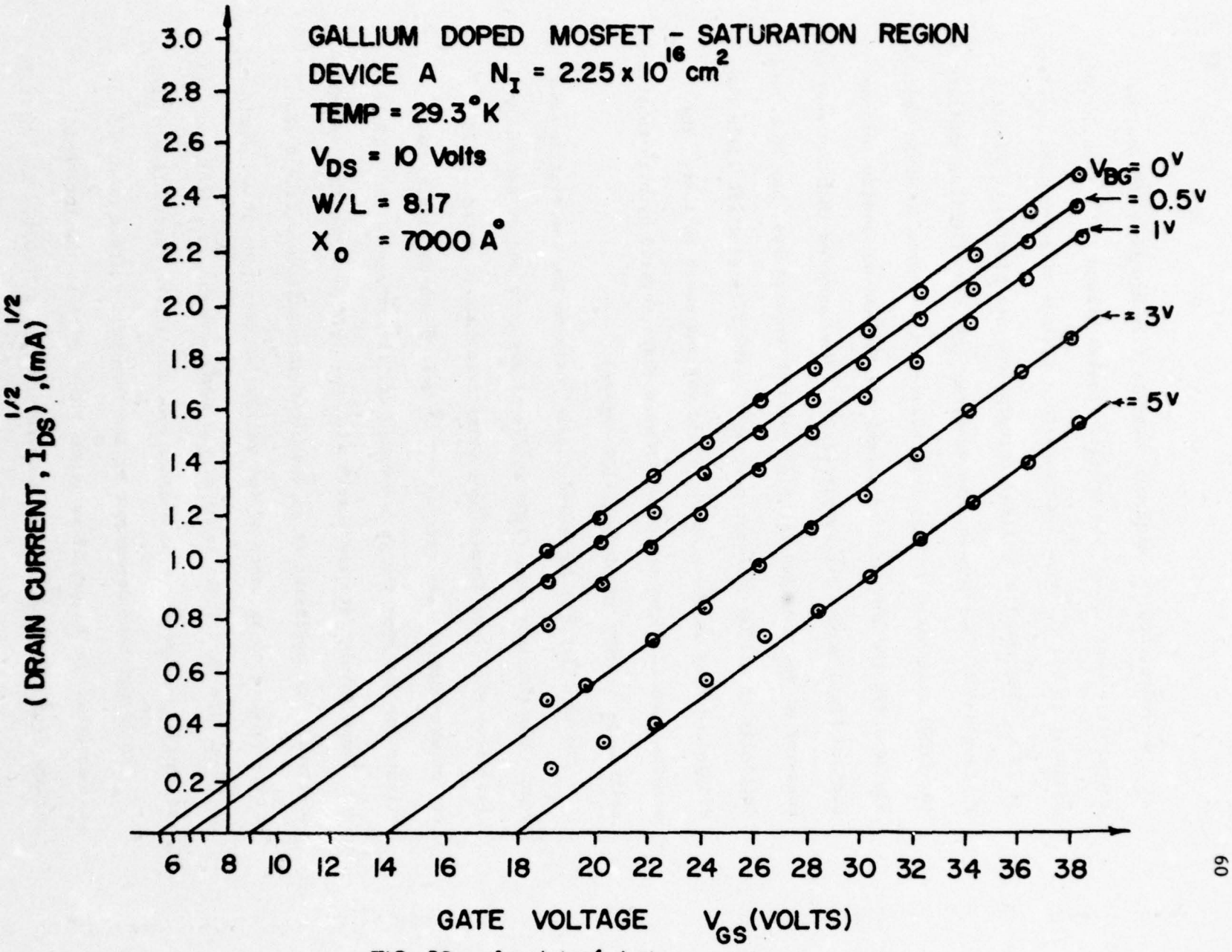

FIG. 29 A plot of drain current versus gate voltage in the saturation region.

the threshold voltage as the temperature is lowered was also observed by C. Rogers [30] , F. Fang and A. Fowler [29] . The threshold voltage is given by equation (6) in the Appendix [27] . From this equation we should conclude that the primary dependence of the threshold voltage on temperature results from Fermi level dependence on temperature. The Fermi potential appears as a part of the surface potential ϕ_s, and the work function ϕ_{ms}, in the above mentioned equation.

If ϕ_s is assumed to be twice the Fermi-potential, and if the dependence of ϕ_{ms} on the Fermi potential is added, then we should expect that the shift in the threshold voltage with temperature should not exceed three times that in the Fermi potential or in other words it should not be more than one volt at the most. However, the observed shift in the threshold voltage is much higher than that (above 20^v between 300^oK and 30^oK). This has also been observed by many researchers, for example [29] , and the shift was attributed primarily to the surface charge in the oxide close to the $Si-SiO_2$ interface. Therefore we will proceed to determine the change in the surface charge w.r.t. a typical value of say $Qss/q - 9 \times 10^{10}/cm^2$, that could have caused the observed shift in the threshold voltage. The procedure for doing this is simply to determine the threshold voltage at the above mentioned typical value for surface charge, then to match this with the measured threshold voltage and hence determine the deviation of the actual surface charge from this typical value. The results of our calculations are plotted on Figure 28.

Another low temperature observation was the hysteresis appearing in the drain characteristics on the curve tracer near 50^oK and low current values. The observed hysteresis virtually disappeared when the gate voltage was doubled. The hysteresis effect was attributed to trapping [30] mechanisms.

We will not attempt to analyze this observation in any detail here.

When the IRFET was triggered by a square wave on the gate, at low temperatures, the rise time of the current between the source and drain was short and temperature independent. The current reached the value I_{DS}^{i} almost instantaneously, with the rising edge of the gate voltage. When the IRFET was turned on with the positive gate voltage, the source to drain current decayed with the thermal time constant, to it's final value I_{DS}^{f}. A voltage proportional to the source to drain current was displayed on the oscilloscope. This voltage was dropped across a 96.8 ohm resistor at the input of the oscilloscope.

The currents I_{DS}^{f} and ΔI_{DS} were measured on Device A, $N_I = 2.25 \times 10^{16}$ cm^{-3}, at various gate to source voltages. The source to drain voltage was kept constant, at $V_{DS} = 10$ V. The measurements were repeated at different temperatures and at different source to drain voltages.

The IRFET photocurrent, $-\Delta I_{DS}$, is shown plotted in Figure 30, as a funtion of V_{GS} in the saturation region, at $V_{DS} = 10$ V, $V_{BG} = 0$, and at $29.4^{o}K$. The plotted line corresponds to the function predicted by equation (25) in the attached appendix.

Calculations based on the measured photocurrent, $-\Delta I_{DS}$, and the measured source to drain current, I_{DS}^{f}, at $29.4^{o}K$ and $V_{DS} = 10$ volt, enabled us to plot the dependence of the initial source to drain current on V_{GS}, Figure 31. This graph shows the dependence of the initial and final source to drain currents on V_{GS}, in the saturation region. The two lines in Figure 31, upper and lower, represent the two charge states of the device, gallium neutral or negative respectively. ΔV_T was determined from Figure 31, it corresponded to 0.9 volt.

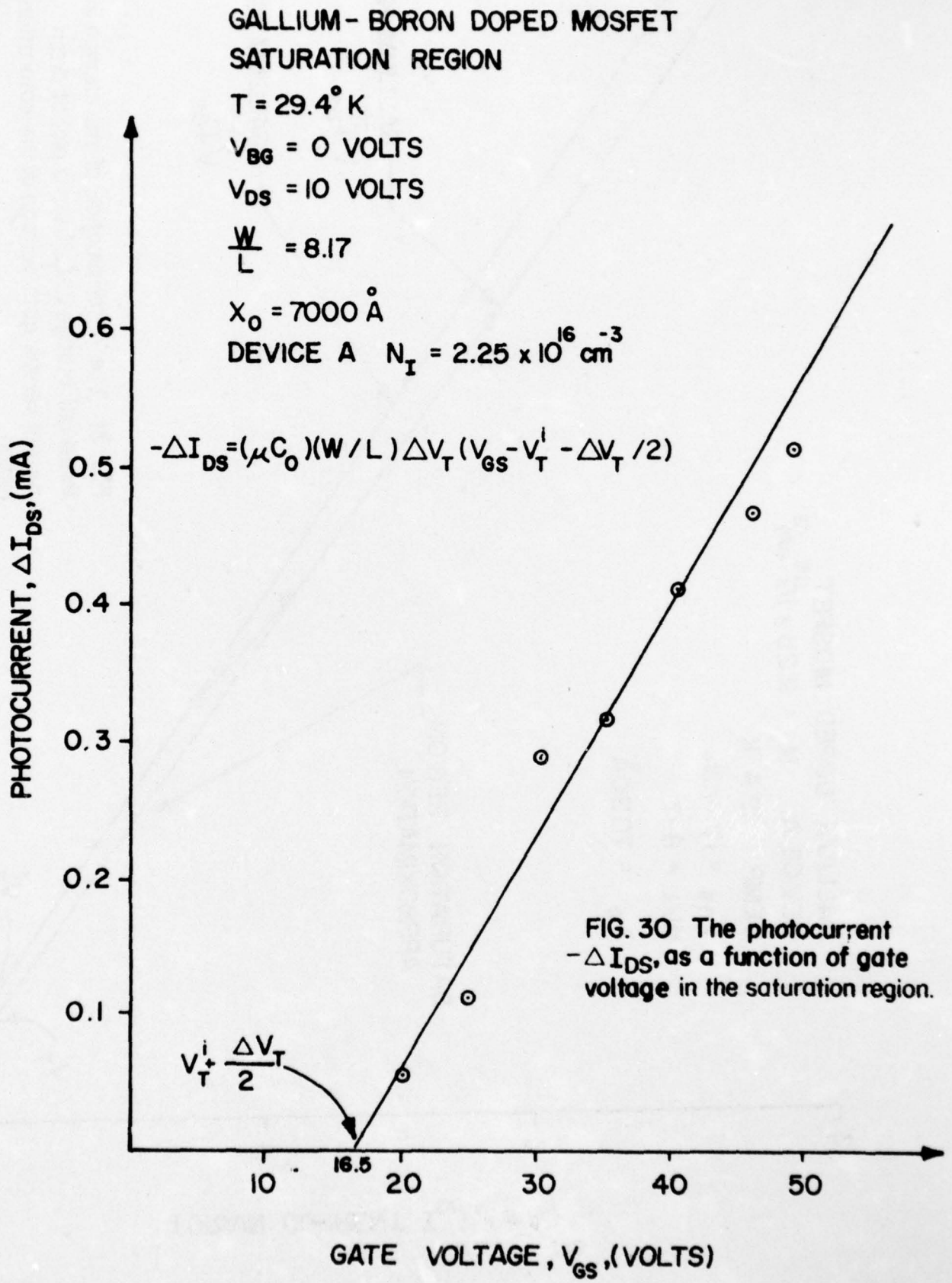

FIG. 30 The photocurrent $-\Delta I_{DS}$, as a function of gate voltage in the saturation region.

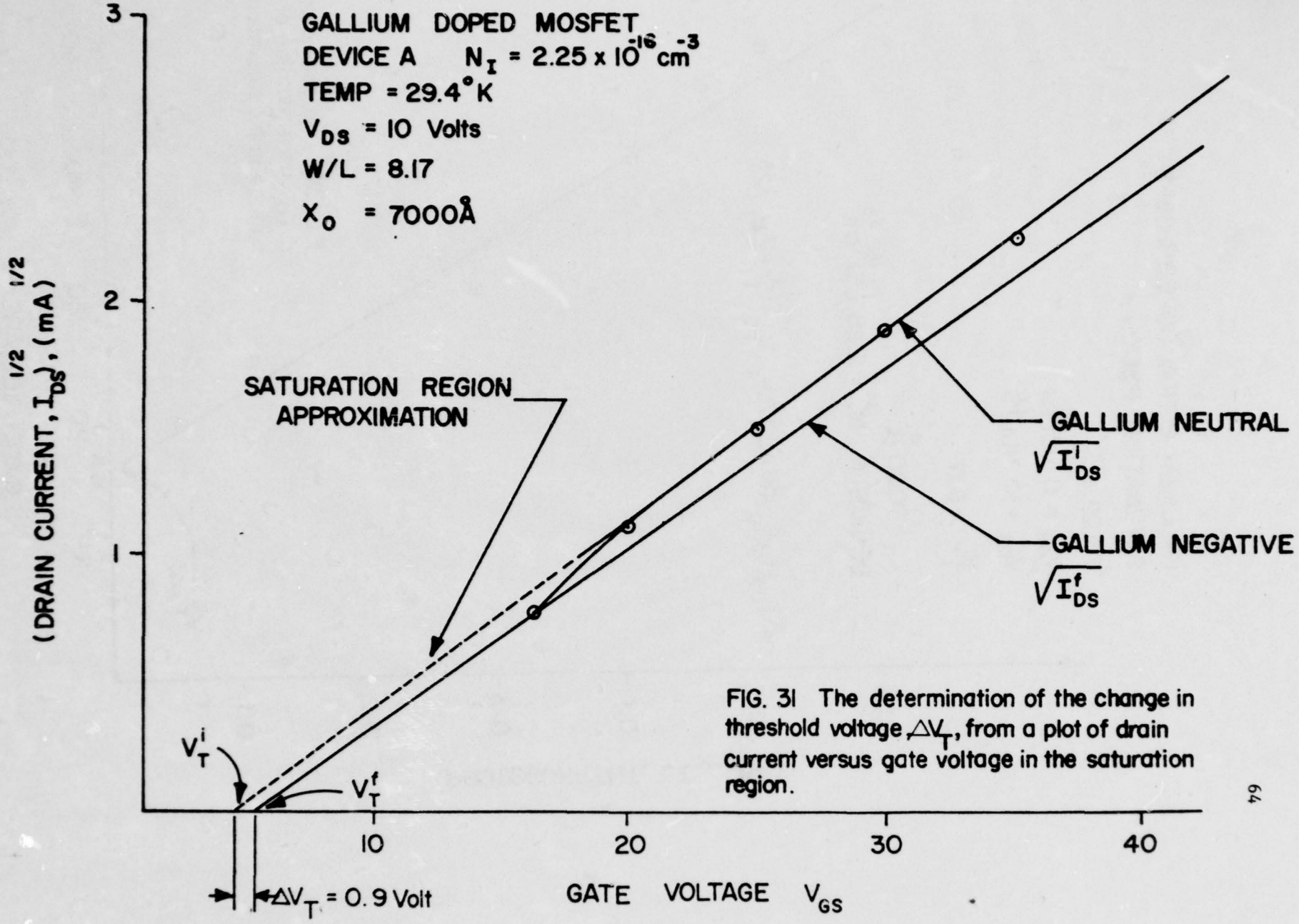

FIG. 31 The determination of the change in threshold voltage, ΔV_T, from a plot of drain current versus gate voltage in the saturation region.

Figure 32, shows the threshold voltage dependence on the $\sqrt{1 + V_{BG}}$, where V_{BG} is the back gate bias potential. The threshold voltage values were determined at the points of intersection of the $\sqrt{I_{DS}^{f}}$ lines with the V_{GS} axis on Figure 31 .

Figure 33 , shows the change in the device threshold voltage between the two charge states as a function of the back gate bias potential. Equation 26, Appendix, was used to calculate the change in the threshold voltage from the measured data , at $V_{BG} = 0$, as follows:

$$\Delta V_T = \frac{(V_{GS} - V_T)}{2} \frac{\Delta I_{DS}}{I_{DS}} \simeq (35/2) \frac{0.43}{6.5} \simeq 1.2 \text{ volts} \qquad (90)$$

The total substrate doping for device A was determined from equation (5) and Figure (19), $N_{sub} = N_I = 2.25 \times 10^{16} cm^{-3}$. The Ga & B concentrations will be calculated from equation 18, Appendix, as follows:

$$\Delta V_T (\text{at } V_{BG} = 0) = \frac{d\,(V_T)}{d\sqrt{1 + V_{BG}}} \left[\frac{1}{2} \left(\frac{N_{GA}}{N_I} \right) \right] \qquad (91)$$

Therefore;

$$1.2 = (12)\ (\tfrac{1}{2})\ \frac{N_{GA}}{2.25 \times 10^{16}} \qquad (92)$$

Therefore;

$$N_{GA} = 0.45 \times 10^{16} cm^{-3} \qquad (93)$$

Therefore;

$$N_A = N_I - N_{GA} = 2.25 \times 10^{16} - 0.45 \times 10^{16}$$

$$= 1.8 \times 10^{16}\ cm^{-3} \qquad (94)$$

The theoretical value of the threshold voltage of the device was determined from the well known MOSFET equations, equations (6) through (11) in the Appendix; the following discussion illustrates the methods we used in this calculation

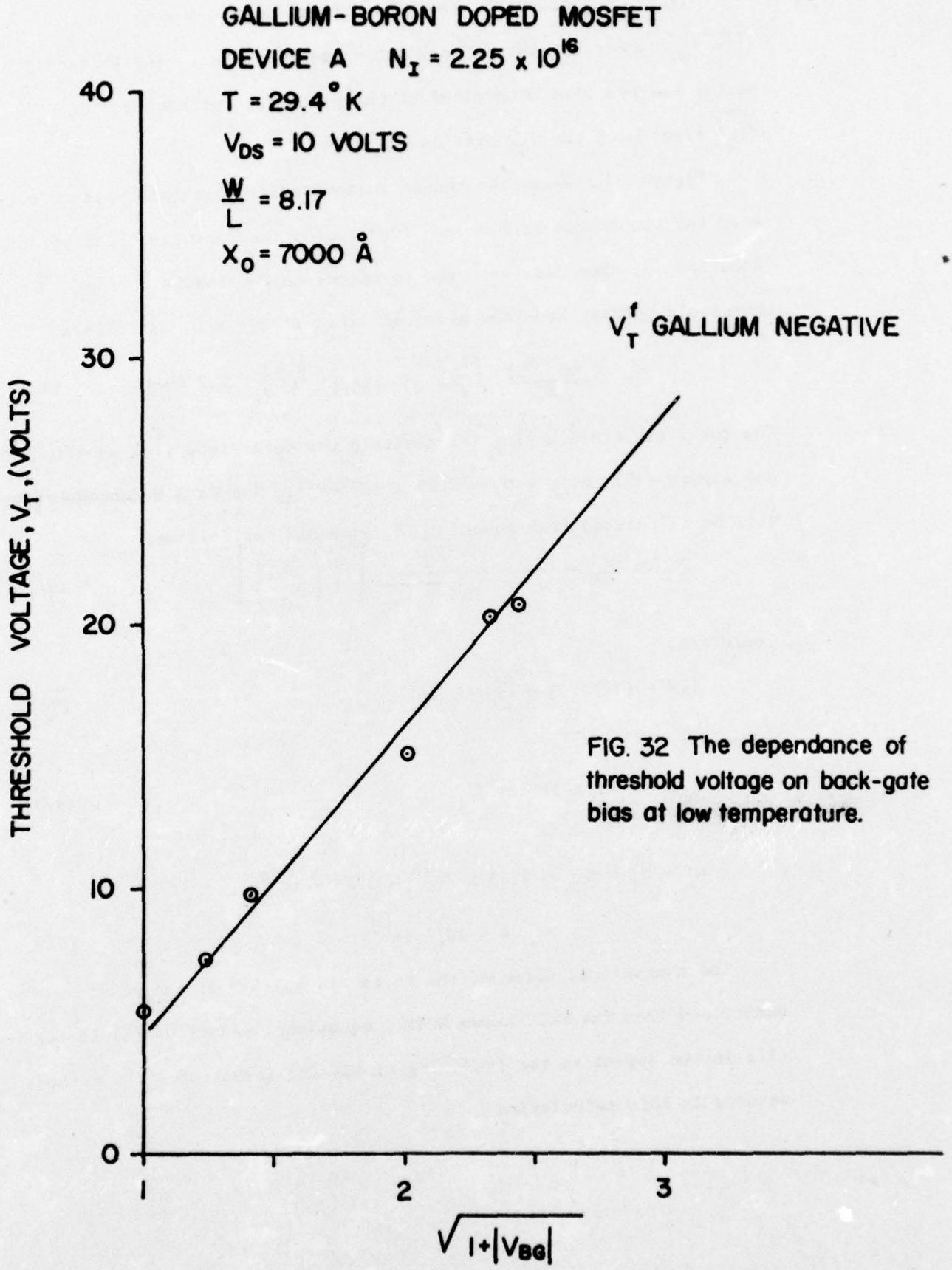

FIG. 32 The dependance of threshold voltage on back-gate bias at low temperature.

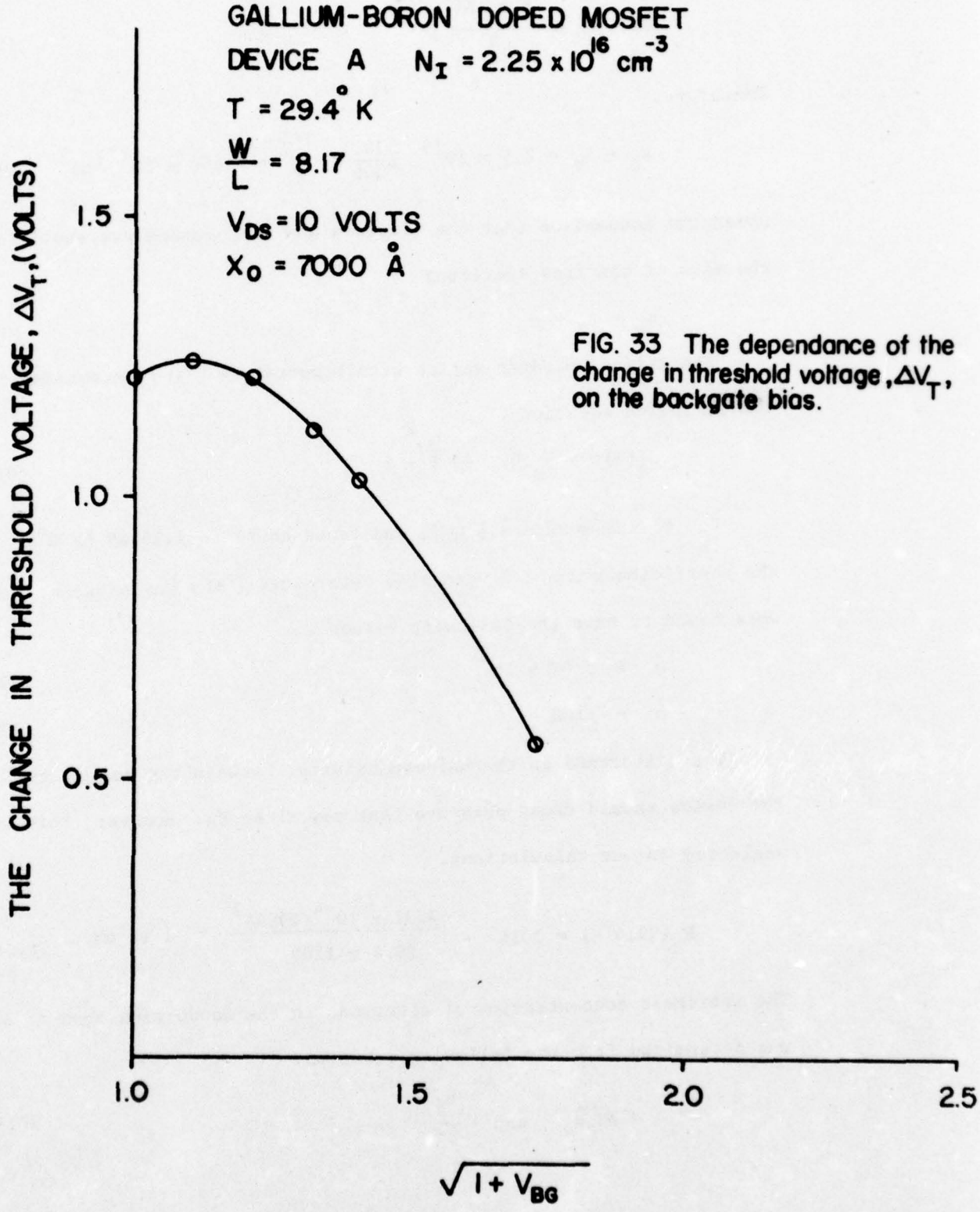

FIG. 33 The dependance of the change in threshold voltage, ΔV_T, on the backgate bias.

The effective density of states in the valence and conduction bands, N_V and N_C were calculated at 29.4°K:

$$N_V = N_C = \left[\frac{2\pi\, m_o\, KT}{h^2}\right]^{3/2} \tag{95}$$

Therefore,

$$N_C = N_V = 2.5 \times 10^{19} \left(\frac{29.4}{300}\right)^{3/2} = 7.669 \times 10^{17}/cm^3 \tag{96}$$

under the assumption that the electron and hole masses are equal to the mass of the free electron:

$$m_e = m_h = m_o \tag{97}$$

The silicon bandgap varies with temperature [31], according to the following equation

$$E_g(T) = E_g(0) - \frac{\alpha T^2}{T + \beta} \tag{98}$$

Eg (0) was measured [32], and found equal to 1.16 eV at 0°K. The coefficients α and β were also determined [31] for silicon, and were found to have the following values

$$\alpha = 7.02 \times 10^{-4} \tag{100}$$

$$\beta = 1108 \tag{101}$$

The difference in thermal expansivity, between the header and the device should cause pressure that may alter Eg. However, this was neglected in our calculations.

$$E_g(29.4^oK) = 1.16 - \frac{7.02 \times 10^{-4}(29.4)^2}{29.4 + 1108} \simeq 1.16 \text{ eV} \tag{102}$$

The intrinsic concentration of electrons in the conduction band at 29.4°K was determined from the following equation:

$$n_i = \sqrt{N_C N_V}\ \exp\left[\frac{-E_g}{KT}\right] \tag{103}$$

Therefore,

$$n_i(29.4^oK) = (7.669 \times 10^{17}) \exp\left[-\frac{1.16}{0.002528}\right]$$

$$\simeq 4X10^{-182}/cm^3 \tag{104}$$

as compared to $1.4 \times 10^{10}/cm^3$ at 300^oK

where

$$\frac{KT}{q} \text{ (at } 29.4^oK) = \frac{KT}{q} \text{ (at } 300^oK) \quad \frac{29.4}{300}$$

$$\frac{KT}{q} = \frac{0.0258}{300} \; 29.4 = 0.002528 \tag{105}$$

The Fermi level ($|\phi_F| = \frac{KT}{q} \ell n \frac{P}{n_i}$), at the temperature of operation lies between the gallium and boron levels. Therefore:

$$\phi_F \simeq \frac{E_g}{2} = \frac{1.16}{2} = -.58eV \tag{106}$$

At this low temperature range, around 29.4^oK, all the boron impurity atoms were still ionized. Therefore, the carrier concentration during the read in period is given by:

$$P \simeq N_I \simeq N_A + N_{GA} \simeq 2.25 \times 10^{16} cm^{-3}. \tag{107}$$

The mobility is known to decrease with the high electric field, where the high electric field operation is defined as $E > 10^3$ V/cm. This is known as the "hot carrier effect". The mobility dependence on temperature and orientation is also complex. Therefore we have used the measured mobility value at this temperature in the model calculations.

$$\mu_e (29.4^oK) = 257.06 \; cm^2/V.sec. \tag{108}$$

The work function between the semiconductor body and the gate field plate was calculated for the Al - SiO_2-Si system, as follows:

$$\phi_{ms} = \phi_m - \phi_s = \phi_{mo} - (\phi_{so} + \frac{E_g}{2q} + \phi_F) \tag{109}$$

$$= 3.2 - (3.25 + \frac{1.16}{2} + 0.58)$$

$$\phi_{ms} = -1.21 \text{ volt} \tag{110}$$

where ϕ_{mo} and ϕ_{so} are the barrier heights between the conduction band of the SiO_2 and both the fermi level of the gate metal, and the silicon conduction band respectively.

The surface charge Q_{ss} at the $Si - SiO_2$ interface is strongly process dependent and may vary with temperature. We have assumed, however, the following typical value:

$$\frac{Q_{ss}}{q} = -9 \times 10^{10}/cm^2 \tag{111}$$

The gate oxide capacitance was calculated from the knowledge of the oxide thickness ($7000A^o$).

$$C_o = \frac{\varepsilon_o K_{ox}}{t_{ox}} = 5.057 \times 10^{-9} \quad F/cm^2 \tag{112}$$

Therefore

$$\frac{-Q_{ss}}{C_o} = \frac{(9 \times 10^{10})(1.6 \times 10^{19})}{5.057 \times 10^{-9}} \simeq -2.84 \text{ volt} \tag{113}$$

The flat band voltage can be determined as follows:

$$V_{FB} = \phi_{ms} - \frac{Q_{ss}}{Co} = -1.21 - 2.84 = -4.05 \text{ volts} \tag{114}$$

From equation (10) in the Appendix, we determine (A),

$$A = V_{FB} + 2\phi_f = -4.05 + 1.16 = 2.89 \text{ volt} \tag{115}$$

Similarily, (B) can determined from equation (11) in the Appendix:

$$B = \frac{\sqrt{2K_{si}\,\varepsilon_o q\,(2\phi_f - V_{BG})}}{C_o} \tag{116}$$

$$= \frac{\sqrt{2 \times 12 \times 8.85 \times 10^{-14} \times 1.6 \times 10^{-19} \times 1.16}}{5.057 \times 10^{-9}}$$

$$B = 1.24 \times 10^{-7} \text{ (at zero back gate bias)} \tag{117}$$

The initial value of the threshold voltage, follows directly from equation (12) in the Appendix.

$$V_T^i = A + B\sqrt{N_A} \tag{118}$$

$$= -2.89 + 1.24 \times 10^{-7}(1.8 \times 10^{16})^{1/2}$$

$$V_T^i \simeq 13.7 \text{ volt} \tag{119}$$

The final value of the threshold, follows from equation (13) in the Appendix:

$$V_T^f = A + B\sqrt{N_A + N_{GA}} \tag{120}$$

$$= -2.89 + 1.24 \times 10^{-7}\left(2.25 \times 10^{16}\right)^{\frac{1}{2}}$$

$$V_T^f = 15.7 \text{ volt} \tag{121}$$

now if we match V_T^i as calculated from equation (119) to that measured we can determine the actual surface charge.

$$\frac{-Qss}{Co} = V_{T\ \text{measured}}^i - \left(V_T^i + \frac{9 \times 10^{10}}{Co} q \right) \tag{122}$$

The initial and final threshold voltages as determined at 29.4°K by extrapolation on Figure 31 were 4.7 and 5.6 volts respectively. Therefore

$$\frac{-Qss}{Co} = 4.7 - \{ 13.7 + 2.84 \} \tag{123}$$

and hence therefore

$$\frac{Qss}{q} = 3.74 \times 10^{11}/cm^2 \tag{124}$$

at 29.4°K

Similarly, the actual surface charge was determined at other temperatures and the result was plotted on Figure 28.

The threshold voltage that was originally negative at room temperature, changed to be a positive quantity at low temperatures, i.e. the depletion device changed to be an enhancement device at low temperatures. No significant changes in the threshold voltage were noticed in the temperature range between 21°K and 35°K.

On Figure 33 we notice that the magnitude of ΔV_T dropped as the back gate bias potential was increased. This is contrary to the behavior that our model suggests. However, the model is only valid for uniformly doped devices. The gallium acculation near the surface

results in a drop in the doping ratio of the depletion region N_{GA}/N_A, as the size of the depletion region increases with the back gate bias. This fact ultimately leads to the reported decrease in ΔV_T as the back gate bias potential is increased.

The change in the threshold voltage ΔV_T, was calculated from equation (25) of the Appendix at $V_{GS} = 40$, $V_T^i + \Delta V_T/2 = 16.5V$ (Figure 30), $W/L = 8.17$, $\mu = 257.06\ cm^2/V.sec$, $Co = 5.057 \times 10^{-9} F/cm^2$ and $\Delta I_{DS} = 0.43\ mA$.

$$-\Delta I_{DS} = \frac{-\mu\ Co\ W}{L} \quad (\Delta V_T) \left(V_{GS} - V_T^i - \Delta V_T/2 \right) \tag{125}$$

Therefore

$$\Delta V_T = 1.2 \text{ volt} \tag{126}$$

This compares very closely to the value of ΔV_T determined by extrapolation of the experimental data on Figure 31.

C. Optical Measurements

When the temperature is around $16^{o}K$, the time constant of thermal ionization of the gallium centers is several seconds long. The optical emission rate at this temperature range is much higher than the thermal emission rate $e_p^o >> e_p^t$.

Where the optical emission rate is defined as

$$e_p^o = \sigma^o \phi \tag{127}$$

σ^o is the photoionization cross section, which is a measure of the probability of carrier emission when photons of a certain frequency are incident on the device, and ϕ is the incident photon flux in number per unit area per second.

The target of the optical measurements, is to verify that the Ga-doped MOSFET can operate as an infrared detector for radiation in the far infrared range (8 - 14 μm), as well as to measure the photoionization cross section of the gallium centers at various frequencies in the far infrared radiation range.

To separate the optical response from the thermal response, the photoionization cross section has to be measured at temperatures around or below $21^{o}K$. At this temperature the thermal decay is negligible.

Our thermal decay measurement reveals that, the activation energy $(E_{Ga} - E_v)$ of the Ga-Center has strong electric field dependence. $E_{Ga} - E_V$ can be varied from 0.071 eV at a field strength of 10^2V/cm to 0.027 ev at 5×10^4 V/cm which is quite different than 0.065 eV given by ref. (16). If the photoionization cross section has the same field dependence, it is conceivable that the spectral response of the Ga-doped MOSFET can be extended well into the infrared by applying a strong electric field. In other words, a tunable infrared

detector can be realized.

In our experiments - so far - we have aimed at a gallium concentration lower or much lower than the boron concentration in the substrate. However, better optical detection and device performance should be expected, when the gallium concentration is much higher than the boron concentration in the substrate. This will obviously increase the photo current, ΔI_{DS}, appreciably.

Although the IRFET can be operated in both the linear and saturation region the responsivity is obviously higher in the saturation region. To illustrate the integration function, which is a property of the IRFET, the photocurrent time dependence in the saturation region is described in the following equation, which compares to equation (25) in the Appendix when $\Delta V_T/2 << V_{GS} - V_T$

$$\Delta I_{DS}(t) = \frac{-\mu C_o W}{L} (\Delta V_T) (V_{GS}-V_T^i) (1-\exp(-t/\tau)) \qquad (128)$$

If the time period $t << \tau$ then equation (128) can be simplified to the following

$$\Delta I_{DS}(t) \simeq \Delta I_{DS} \frac{t}{\tau} \qquad (129)$$

Therefore, the IRFET integrates the incident photon radiation in the time period $t << \tau$. The total input energy is therefore expressed as follows [7]

$$E_{in} = \Phi . t . \hbar\omega . A \qquad (130)$$

where

$\hbar = \frac{h}{2\pi}$, where h is the Plank constant = 6.625×10^{-34} Joule. second.

$\omega = 2\pi\nu$ where ν is the frequency of the incident radiation.

A is the active area of the device = WL

The output power at the end of the integration period t ($t<<\tau$), is

given by (7)

$$P_{out} = \left|\Delta I_{DS}(t)\right| . \ V_{DS} \tag{131}$$

The responsivity will be defined as (7)

$$\text{Responsivity} = \frac{\text{Output Power}}{\text{Input Energy}} \tag{132}$$

$$R = \frac{|\Delta I_{DS}(t)| . V_{DS}}{\Phi . t. \hbar w . A} \tag{133}$$

The responsivity, according to the above definition, can be increased by increasing the drain voltage and reducing the active area while keeping the W/L ratio constant (7).

D. Performance

In this section we will attempt to calculate a typical value for the responsivity of a Ga-B doped IRFET. The device will be assumed to have the following specifications

$W/L = 8$, $A = 2.5 \times 10^{-3} cm^2$, $X_o = 7000\ A^o$

The input energy can be calculated from equation (130)

$$E_{in} = \Phi . t . \hbar\omega . A, \tag{134}$$

The photon energy at 11 μ meter is given by

$$\hbar\omega = h\nu = h\frac{c}{\lambda} = \frac{6.25 \times 10^{-34} \times 3 \times 10^{10}}{1.6 \times 10^{-19} 11 \times 10^{-4}} = 0.1073V \tag{135}$$

if

$\Phi = 10^{16}$ #/cm^2 sec and t = 500 milli sec

Then the input energy can be calculated as follows

$$E_{in} = 10^{16} \times 0.5 \times -.107 \times 1.6 \times 10^{-19} \times 2.5 \times 10^{-3}$$

$$= 2.14 \times 10^{-7} \text{ Joules} \tag{136}$$

The output power = $|\Delta I_{DS}| \times V_{DS}$

$$= 0.55 \times 10 = 5.5 \text{ milli Watts} \tag{137}$$

Therefore the responsivity can be determined as follows

$$\text{Responsivity} = \frac{\text{Output Power}}{\text{Input Energy}} = \frac{5.5 \text{ milli Watts}}{0.214 \text{ micro Joule}}$$

$$= 25.7 \text{ m W/}\mu \text{ Joule} \tag{138}$$

VI. CONCLUSIONS

A process for fabricating the gallium-boron doped MOSFET has been developed. The gallium was diffused in the wafer through a silicon dioxide layer [33].

The ionization energy of the gallium center was measured at low temperature in the depletion region of a MOSFET behind a strongly inverted channel. The thermal activation energy of the gallium center was measured and found less than the previously reported ionization energy of gallium [16,19,20]. The reduction in the ionization energy was attributed to the barrier lowering as a result of the MOSFET's surface potential. The Poole-Frenkel model [9] was used in the data analysis. It was found that the barrier lowering calculated from this model is comparable to the difference between the previously reported gallium ionization energy [19] and the measured thermal activation energy.

A solution of Poisson's equation in the depletion region of the MOSFET suggests that part of the gallium population in the depletion region may be permanently ionized at any low temperature by the electric field.

The mobility and threshold voltage temperature dependance that were observed, were consistent with the low temperature observations of others [29,30]. The observed shift in the threshold voltage was attributed to changes in the surface charge.

The IRFET model, previously suggested [2] was found to describe the Ga-doped IRFET operation with accuracy sufficient for most engineering applications.

REFERENCES

1. L. Forbes and J. R. Yeargan, "Design for Silicon Infrared Sensing MOSFET," IEEE Trans. Electron Devices, Vol, ED-21, No. 8, pp 459-462, August 1974.

2. W. C. Parker and L. Forbes, "Experimental Characterization of Gold-Doped Infrared-Sensing MOSFET's." IEEE Trans. Electron Devices, Vol. ED-22, No. 10, October 1975.

3. W. C. Parker, L. L. Wittmer, J. R. Yeargan and L. Forbes, "Experimental Characterization of Infrared Response of Gold-Doped Silicon MOSFET's (IRFETs)," presented as paper 4.8 at International Electron Device Meeting, Washington, D. C., Dec. 1974.

4. R. Newman, "Optical Properties of Indium-Doped Silicon," Phys. Rev., Vol. 99, No. 2, pp 465-467, 1955.

5. L. L. Wittmer, W. C. Parker, H. Elabd, K. W. Loh, J. R. Yeargan and L. Forbes, "The Infrared Sensing MOSFET," presented as paper 22.5 at International Electron Device Meeting, Washington, D. C., December 1975.

6. J. C. Fraser and D. H. Alexander, "An Extrinsic Silicon Charge Coupled Device for Detecting Infrared Radiation," presented as paper at International Electron Device Meeting, Washington D. C., December 1974.

7. W. C. Parker, "Experimental Characterization of Gold-Doped Infrared-Sensing MOSFET's," M. S. Thesis, University of Arkansas, Fayetteville, 1975.

8. M. Martini and T. A. McMath, "Field Dependance of the Capture and Re-emission of Charge Carriers by Shallow Levels in Germanium and Silicon." Solid-State Electronics, 1973, Vol. 16 pp 129-142.

9. J. R. Yeargan and H. L. Taylor, "The Poole-Frenkel Effect with Compensation Present." J. of Applied Physics, Vol. 39, No. 12, 5600-5604, November 1968.

10. See for example, A. S. Grove, Physics and Technology of Semiconductor Devices, Wiley, 1967, Chapter 3.

11. Mil[illegible] Genser, Emulsitone Company, private communication.

12. SZE, Physics of Semiconductor Devices, Wiley-Interscience, 1969.

13. A. G. Milnes, "Deep Impurities in Semiconductors," A Wiley-Interscience Publication, John Wiley & Sons, 1973. Chapter 1, 5, 7 and 10.

14. W. Kohn, "Shallow Impurity States in Silicon and Germanium," Solid State Phys., 5, (1957).

15. P. P. Debye and E. M. Conwell, Phys. Rev. 93, 693 (1954).

16. F. J. Morin, J. P. Maita, R. G. Shulman and N. B. Hannay, Phys. Rev. 96, 833 (1953)

17. T. H. Geballe and F. J. Morin, Phys. Rev. 95, 1085 (1954)

18. W. Shockley, "Electrons and Holes in Semiconductors," Section 16.4. Van Nostrand New York, 1950. (U of A Library QC 721S52).

19. E. Burstein, G. S. Picus, B. Henvis, and R. Wallis, J. Phys. Chem. Solids 1, 65 (1956). "Absorption Spectra of Impurities in Silicon-I-Group III Acceptors."

20. G. S. Picus, E. Burstein, and B. Henvis, J. Phys. Chem. Solid 1, 75 (1956). Journal of the Physics and Chemistry of Solids. "Absorption Spectra of Impurities in Silicon-II-Group V Donors."

21. V. L. Yen, "Circular Variable Filter," Optical Spectra. Reprint was obtained from the manufacturer. Optical Coating Laboratories Inc. OCLI.

22. "Laboratory Cryogenic Systems," Manufacturer's Catalog No. LCS-873/5M. Air Products and Chemicals, Inc.

23. "Cryo-Tip Instruction and Operating Manual," Manufacturer's Handbook of Model AC-2 Cryo-Tip. (June 1967).

24. A. G. Koury, Air Products and Chemicals Inc., private communication.

25. W. Shockley and W. T. Read, Jr., "Statistics of the Recombinations of Holes and Electrons," Physc. Rev., Vol. 87, No. 5, Sept 1, 1952.

26. C. T. Sah, "The Equivalent Circuit Model in Solid-State Electronics," "Part I: The Single Energy Level Defect Centers," Proc. IEEE, Vol. 55, pp 654-671, May 1967.

27. W. N. Carr, J. P. Mize, R. E. Sawyer and J. R. Miller, "MOS/LSI Design and Application," 1972, McGraw-Hill Book Company.

28. D. Frohman - Bentchkowsky and A.S. Grove, "Conductance of MOS-Transistors in Saturation," IEEE Trans. Electron Devices, Vol. Ed. - 16, p. 100, 1969.

29. F. F. Fang and A. B. Fowler, "Transport Properties of Electrons in Inverted Silicon Surfaces." Phys. Rev., Vol. 169, Number 3, 15 May 19769.

30. C.G. Rogers, "MOST's at Cryogenic Temperatures" Solid State Elect., Vol. 11 pp. 1079 - 1091, 1968.

31. Vershni "Temperature Dependence of the Energy Gap in Semiconductors," Physics, 34, 149, (1967).

32. T.P. Mclean., "Prog. in Semiconductors" Heywood & Co. Ltd., London, 1960.

33. A. S. Grove, O. Leistiko, Jr. and C.T. Sah, "Diffusion of Gallium Through a Silicon Dioxide Layer" J. Phys Chem. Solids, Pergamon Press 1964. Vol. 25, pp. 985 - 992.

APPENDIX

W. C. Parker and L. Forbes [2] have presented a model of the IRFET operation. The gallium-boron double doped MOSFET responce data was found in quite good agreement with that predicted by theory. The model equations are summarized here for easy reference. The equations were also modified to fit the operation of the double doped gallium-boron N-channel MOSFET.

To explain the phenomena of the modulation of the channel conductance by the infrared radiation at low temperatures mathematically, we will start by stating the charge neutrality condition,

$$Q_G + Q_{SS} = - (Q_{CH} + Q_{Ga} + Q_B) \qquad (1)$$

where Q_G is the charge on the gate, Q_{SS} is the fixed positive surface state charge at the silicon-silicon dioxide interface, Q_{CH} is the charge contributed by carriers in the channel, Q_{Ga} is the charge of ionized gallium atoms in the oxide or near the silicon surface, and Q_B is the charge in the surface depletion region.

When the gallium centers in the depletion region are photoionized, the net space charge, Q_B, becomes more negative, and the MOSFET has to lose electrons from the channel to reduce the channel charge, Q_{CH}, and maintain neutrality. This results in a corresponding decrease in the magnitude of the drain current. All other terms in equation (1) are constants.

1. The Time Constants of the Device

The thermal time constant will be referred to as τ_t, and will be defined as the reciprocal of the thermal emission rate, e_p^t. Similarly the optical time constant will be referred to as τ_o, and will be defined as the reciprocal of the optical emission rate, e_p^o.

$$\tau_t = \frac{1}{e_p^t} \quad , \quad \tau_o = \frac{1}{e_p^o} \qquad (2), (3)$$

2. The Effective Doping of the P-Type Substrate

N_I is the effective doping of the P-type substrate, N_A is the boron concentration, and N_{Ga} is the gallium concentration.

(a) During the reset operation with the accumulation voltage applied:

Since the gallium centers are neutral, then

$$N_I = N_A \qquad (4)$$

(b) The condition during the read-in period or the device effective doping after the photoionization:

Since the gallium centers are negative, then

$$N_I = N_A - N_{Ga} \qquad (5)$$

3. The Threshold Voltage

For an n-channel MOSFET, the threshold voltage is given by [27]

$$V_T = V_{FB} + 2\phi_F + \frac{Q_B}{C_o} \qquad (6)$$

where V_{FB} is the gate voltage required to establish the flat band condition, ϕ_F is the Fermi potential, C_o is the gate oxide capacitance/unit area, and Q_B is the depletion layer charge generated by the ionized impurity atoms.

$$Q_B = \sqrt{2\kappa_{Si}\varepsilon_o q N_I (2\phi_F - V_{BG})} \qquad (7)$$

Where κ_{Si} is the relative dielectric constant of silicon, ε_o is the electric permitivity of free space, q is the electronic charge, and V_{BG} is the back gate bias potential: a reverse bias on the substrate that increases the electric field in the depletion region and ionizes additional impurity centers.

substituting equation (7) into equation (6), we obtain

$$V_T = V_{FB} + 2\phi_f + \frac{\sqrt{2\kappa_{Si}\epsilon_o q[2\phi_F - V_{BG}]}}{C_o}\sqrt{N_I} \tag{8}$$

Equation (8) can also be expressed as follows:

$$V_T = A + B\sqrt{N_I} \tag{9}$$

where

$$A = V_{FB} + 2\phi_F, \tag{10}$$

and

$$B = \frac{\sqrt{2\kappa_{Si}\epsilon_o q[2\phi_F - V_{BG}]}}{C_o} \tag{11}$$

A and B will be assumed constants for a device at constant temperature and constant back gate bias operating conditions. The only term that may vary is ϕ_F since it is dependent on doping. However, for $V_{BG} > 2\phi_f$ our assumption will still be accurate.

(a) The threshold voltage during the reset operation with the accumulation voltage applied (initial condition);

$$V_T^i = A + B\sqrt{N_A} \tag{12}$$

as obtained from substituting Equation (4) into Equation (9).

(b) The threshold voltage after the photoionization (final condition);

by substituting Equation (5) into Equation (9) we get;

$$V_T^f = A + B\sqrt{N_A + N_{Ga}} \tag{13}$$

Hence, the increase in the threshold voltage is

$$\Delta V_T = V_T^f - V_T^i = B(\sqrt{N_A + N_{Ga}} - \sqrt{N_A}) \tag{14}$$

$$\Delta V_T = B \left[\sqrt{1 + \frac{N_{Ga}}{N_A}} - 1\right] \sqrt{N_A} \tag{15a}$$

for the case that $N_{Ga} << N_A$; we (15b)

$$\Delta V_T = B\sqrt{N_A}(1 + (N_{Ga}/2N_A) - 1) = \frac{BN_{Ga}}{2\sqrt{N_A}}$$

(c) The variation of the threshold voltage as a function of the back gate bias potential;

differentiating equation (9), under the assumption that $2\phi_f = 1$;

$$\frac{d(V_T)}{d[\sqrt{1 + |V_{BG}|}]} = B\sqrt{N_I} \tag{16a}$$

or:

$$B = \frac{1}{\sqrt{N_I}} \left[d(V_T)/d(\sqrt{1 + V_{BG}})\right] \tag{16b}$$

Equation (15b) for the case that $N_{Ga} << N_A$, can be expressed in terms of the effective doping N_I as shown in equation (17)

$$\Delta V_T = B \frac{1}{2} \frac{N_{GA}}{\sqrt{N_I}} \tag{17}$$

Substituting equation (16b) into equation (17), and assuming $N_{Ga} << N_A$ we obtain

$$\Delta V_T \simeq \frac{d(V_T)}{d[\sqrt{1 + V_{BG}}]} \frac{1}{2} \frac{N_{GA}}{N_I} \tag{18}$$

In other words, the gallium concentration in the device can be determined from the measurement of ΔV_T at a certain back gate bias potential and from the measurement of the V_T dependance on the Back gate bias potential.

4. The Time Dependance of the Ionization Process: The number of Ga centers in the negative charge state N_T is given by:

$$N_T(t) = N_{Ga}[1 - e^{-t/\tau_o}] \tag{19}$$

under the assumption that

$$\tau_t >> \tau_o \text{ at the temperature of operation.}$$

Where $N_T(t)$ is the total number of the ionized gallium centers at time t.

5. The Time Dependance of the Threshold Voltage

From equation (15-a) and (19), we obtain

$$V_T^L = V_T^i + \Delta V_T(t)$$

$$= V_T^i + B\sqrt{N_A}\left[\sqrt{1 + \frac{N_{Ga}}{N_A}[1 - e^{-t/\tau_o}]} - 1\right] \tag{20}$$

where $V_T^L(t)$ is the threshold voltage as a function of the illumination time.

6. MOSFET Current-Voltage Equation in the Linear Region

The linear region is defined in the well known [27] MOSFET model as the region of the I-V Characteristics where

$$V_{GS} - V_T > V_{DS} \ .$$

Therefore the source to drain current I_{DS} in the linear region is

$$I_{DS} = \frac{\mu C_o W}{2L}[2V_{DS}(V_{GS} - V_T) - V_{DS}^2] \tag{21}$$

where μ is the carrier mobility at the surface, $\frac{W}{L}$ is the channel width to length ratio, V_{DS} is the drain to source voltage, and V_{GS} is the applied gate voltage.

7. MOSFET Current Voltage Equation in the Saturation Region

For $V_{DS} > V_{Gs} - V_T$, the MOSFET is operating in the saturation region. In this case (27)

$$I_{DS} = \frac{\mu C_o W}{2L} (V_{GS} - V_T)^2 \qquad (22)$$

C_o in equations (21) and (22) is the oxide capacitance per unit area. C_o can be determined from the parallel plate capacitance equation.

$$C_o = \kappa_{ox} \varepsilon_o / t_{ox} \qquad (23)$$

where κ_{ox} is the dielectric constant of the oxide and t_{ox} is the oxide and t_{ox} is the oxide thickness under the gate.

8. The Photocurrent

The photocurrent ΔI_{DS} is the change in the source to drain current as a result of the photoionization. ΔI_{DS} can be expressed in terms of the change in the threshold voltage ΔV_T for both the linear and saturation regions.

For the linear region from equation (21), for a given V_{DS}

$$\Delta I_{DS} = \frac{-\mu C_o W}{L} (\Delta V_T)(V_{DS}) \qquad (24)$$

For the saturation region from equation (22)

$$\Delta I_{DS} = \frac{-\mu C_o W}{L} (\Delta V_T) (V_{GS} - V_T - \Delta V_T/2) \qquad (25)$$

The negative sign in the two above equations indicates that the source to drain current decreases after illumination. Dividing equation (25) by equation (22), we have:

$$\frac{\Delta I_{DS}}{I_{DS}} = - \frac{(2 \Delta V_T)}{V_{GS} - V_T} \qquad (26)$$

in the saturation region.

9. The Current-Time Dependance

From equations (20), (24), and (25) we obtain for the linear region:

$$I^{L}_{DS}(t) = \frac{+\mu C_o W}{L} V_{DS} \left(V_{GS} - V^{i}_{T} - B\sqrt{N_A} \left[\sqrt{1 + \frac{N_{Ga}[1 - \exp -t/\tau_o]}{N_A}} - 1\right] - \frac{V_{DS}}{2}\right] \quad (27)$$

For the saturation region:

$$I^{L}_{DS}(t) = \frac{+\mu C_o W}{2L} \left[V_{GS} - V^{i}_{T} - B\sqrt{N_A} \left[\sqrt{1 + \frac{N_{Ga}[1 - \exp \frac{-t}{\tau o}]}{N_A}} - 1\right]\right]^2 (28)$$

Equations (27) and (28) express the source to drain current as a function of the illumination time. The time $t = 0$, corresponds to the beginning of the ionization process.

10. <u>The time dependance of the threshold voltage and drain current when the $N_{Ga} << N_A$ & $\Delta I_{DS} << I_{DS}$:</u>

If $N_{Ga} << N_A$, equation (20) can be simplified using the binomial approximation.

$$V^{L}_{T}(t) \simeq V^{i}_{T} + \frac{BN_{Ga}}{2\sqrt{N_A}} (1 - e^{-t/\tau_o}) \quad (29)$$

From equation (21) and equation (24), by algebraic manipulation we obtain the following equation

$$\Delta V_T = - \frac{\Delta I_{DS}}{I_{DS}} (V_{GS} - V_T - V_{DS/2}) \quad (30)$$

in the linear region and similarly from the equations (22) and (25) we obtain

$$\Delta V_T = (V_{GS} - V_T)\left(1 - \sqrt{1 + \Delta I_{DS}/I_{DS}}\right) \tag{31}$$

in the saturation region.

If $\Delta I_{DS} \ll I_{DS}$, then equation (31) can be simplified to the following

$$\Delta V_T \simeq \frac{\Delta I_{DS}}{2I_{DS}} (V_{GS} - V_T) \tag{32}$$

again in the saturation region.

Equations (27) and (28) can in turn be simplified when $N_{Ga} \ll N_A$, they lead to equations (33) and (34) respectively.

$$I_{DS}^{L}(t) = \frac{\mu C_o W}{L} V_{DS}\left(V_{GS} - V_T^i - B\frac{N_{Ga}}{2\sqrt{N_A}}(1 - \exp(-t/\tau_o)) - V_{DS}/2\right) \tag{33}$$

$$I_{DS}^{L}(t) = \frac{\mu C_o W}{2L} \left(V_{GS} - V_T^i - \frac{BN_{Ga}}{2\sqrt{N_A}}(1 - \exp(-t/\tau_o))\right)^2 \tag{34}$$

MISSION
of
Rome Air Development Center

RADC plans and conducts research, exploratory and advanced development programs in command, control, and communications (C^3) activities, and in the C^3 areas of information sciences and intelligence. The principal technical mission areas are communications, electromagnetic guidance and control, surveillance of ground and aerospace objects, intelligence data collection and handling, information system technology, ionospheric propagation, solid state sciences, microwave physics and electronic reliability, maintainability and compatibility.

Printed by
United States Air Force
Hanscom AFB, Mass. 01731